Fracture behaviors of tough adhesive hydrogels

by

Xiang Ni

Department of Mechanical Engineering
McGill University, Montreal, Quebec, Canada
April 2021

A thesis submitted to McGill University in partial fulfillment of the requirements for the degree of Master of Engineering.

Abstract

Tough adhesive hydrogels find increasing use in engineering and medicine by virtue of high toughness of matrix and strong adhesion to diverse substrates. In many applications, tough adhesive hydrogels are exposed to various environmental and loading conditions. One example is prolonged cyclic loading when the hydrogels are used as tissue adhesives interfacing with repeatedly deforming tissues such as heart and lung. Another example is swelling when implanted hydrogels contacting with body fluids, which deteriorate mechanical performance. Although hydrogel adhesion has been studied, how the tough adhesive hydrogels behave under cyclic loading and upon swelling remains elusive. In this thesis, a combination of experimental, computational and analytical methods is deployed to address these questions. First, modified lap-shear tests are applied to exert three types of loading (monotonic, static, and cyclic loads) to tough adhesive hydrogels. The results show two interfacial fracture phenomena: fast debonding and interfacial fatigue fracture. The existence of interfacial fatigue threshold is confirmed and compared with theoretical calculation and fatigue of bulk hydrogels. To investigate how fracture properties of tough adhesive hydrogels evolve with swelling process, tough adhesive hydrogels are swollen controllably for varying polymer fractions and characterized for their cohesion and adhesion energies, respectively. The results show a similar scaling law (ϕ^{v}) of these two quantities as a function of the polymer fraction (ϕ). The results are further analyzed through scaling analysis and finite element simulation, finding that it stems from the scaling of shear modulus. This thesis will advance the fundamental understanding of tough adhesive hydrogels, promote investigation on fracture of hydrogel adhesion, and motivate the development of next-generation tissue adhesives.

RÉSUMÉ

Les hydrogels adhésifs résistants trouvent une utilisation croissante dans l'ingénierie et la médecine en raison de la ténacité élevée de la matrice et de la forte adhérence à divers substrats. Dans de nombreuses applications, les hydrogels adhésifs résistants sont exposés à diverses conditions environnementales et de charge. Un exemple est le chargement cyclique prolongé lorsque les hydrogels sont utilisés comme adhésifs tissulaires s'interfaçant avec des tissus à déformation répétée tels que le cœur et les poumons. Un autre exemple est le gonflement lorsque des hydrogels implantés entrent en contact avec des fluides corporels, ce qui détériore les performances mécaniques. Bien que l'adhérence des hydrogels ait été étudiée, le comportement des hydrogels adhésifs résistants sous charge cyclique et lors du gonflement reste insaisissable. Dans cette thèse, une combinaison de méthodes expérimentales, computationnelles et analytiques est déployée pour répondre à ces questions. Tout d'abord, des tests de cisaillement par recouvrement modifiés sont appliqués pour exercer trois types de charges (charges monotones, statiques et cycliques) sur des hydrogels adhésifs résistants. Les résultats montrent deux phénomènes de fracture interfaciale : le décollement rapide et la fracture de fatigue interfaciale. L'existence d'un seuil de fatigue interfaciale est confirmée et comparée au calcul théorique et à la fatigue des hydrogels en vrac. Pour étudier comment les propriétés de rupture des hydrogels adhésifs durs évoluent avec le processus de gonflement, les hydrogels adhésifs durs sont gonflés de manière contrôlée pour différentes fractions de polymère et caractérisés pour leurs énergies de cohésion et d'adhérence, respectivement. Les résultats montrent une loi d'échelle (ϕ^{ν}) similaire de ces deux quantités en fonction de la fraction de polymère (ϕ). Les résultats sont ensuite analysés par une analyse de mise à l'échelle et une simulation par éléments finis, concluant qu'ils découlent de la mise à l'échelle du module de cisaillement. Cette thèse fera progresser la compréhension fondamentale des hydrogels adhésifs résistants, favorisera l'étude de la fracture de l'adhésion des hydrogels et motivera le développement d'adhésifs tissulaires de nouvelle génération.

Acknowledgements

First, I would like to thank my supervisor, Professor Jianyu Li. Thank you for supervising me in three years and taking me to the academic ride. Your research philosophy and attitude deeply affect me and will continue to illuminate my future academic path.

I would also like to acknowledge my outstanding colleagues in the lab for their wonderful collaboration. Particularly, I appreciate the kind support from Zhen Yang and Guangyu Bao. I will always remember the happy memories created in the lab, in the office and on dining tables.

Finally, I would like to thank my parents for their love and support. I always feel you are on my side. I can not pursue my academic dream without your backup. Thank you for everything you have done for me.

Table of Contents

List of Tables and Figures

Contribution of Authors

In chapter 3 article 1 (Ni, X., Chen, C., & Li, J. (2020). Interfacial fatigue fracture of tissue adhesive hydrogels. *Extreme Mechanics Letters*, 34, 100601.), Xiang Ni and Jianyu Li conceived and designed the study. Xiang Ni conducted all the experiments. Chao Chen and Jianyu Li developed the theoretical framework to calculate the energy release rate. Xiang Ni, Chao Chen and Jianyu Li analyzed the results and wrote the manuscript.

In chapter 4 article 2 (Ni, X., Yang, Z., & Li, J. (2021). Scaling behavior of fracture properties of tough adhesive hydrogels. *ACS Macro Letters*, 10(2), 180-185.), Xiang Ni and Zhen Yang contributed equally. Xiang Ni performed experiments and Zhen Yang conducted simulation. Xiang Ni, Zhen Yang and Jianyu Li conducted the analysis. Jianyu Li supervised the project. All authors contributed to and approved the manuscript.

Chapter 1. Introduction

1.1. Background

Hydrogel tissue adhesives are promising in surgical purposes, since they can provide wound closure and hemostasis while controlling drug delivery and preventing fluid leakage [1]. Compared with traditional wound dressing methods, such as suturing and stapling, hydrogel tissue adhesives have several remarkable advantages, including easy using, rapid working and less secondary damaging [2]. Thus, hydrogel tissue adhesives are increasingly used in many branches of medicine.

Despite their versatile applications, hydrogel tissue adhesives still have several unsolved issues, in particular limited mechanical properties [3], which directly determine their performance. Thus, commercial hydrogel tissue adhesives are still limited in clinical use to date.

Recently developed tough adhesive hydrogels successfully overcome these problems by virtue of superior toughness of hydrogel matrix and strong adhesion to diverse tissue [4, 5]. Inspired by tough adhesive hydrogels, a series of tissue adhesives with superior mechanical properties are invented, such as photo-controllable adhesives [6], degradable adhesives [7], and thermo-responsive adhesives [8]. All these adhesives would open a plethora of applications where tissue adhesives should withstand repeated stress arising from dynamic movement of tissue.

The capacity to sustain cyclic loading is mission-critical for tough adhesive hydrogels since many organs and tissue are always in repeatedly deformed state in human body. For example, a heart beats 60 to 100 times per minute [9] and tendon is stretched in every step when we walk [10]. To apply tough adhesive hydrogels in these scenarios, for instance, sealing a wound on a beating heart and repairing an injured tendon, it is necessary to study fracture behaviors of tough adhesive hydrogels under prolonged cyclic loading, i.e., interfacial fatigue fracture.

While fracture mechanics of tough hydrogel adhesion has been explored, previous research mainly focuses on monotonic loading [4]. Also, recent studies on fatigue fracture of hydrogels investigate bulk failure rather than interfacial failure [11-13], thereby leaving a gap on the response of tough adhesive hydrogels under cyclic loading.

Another key challenge posed by hydrogel adhesive applications is swelling and following deterioration of mechanical properties. Because human body is full of body fluids, implanted hydrogel adhesives would readily contact with fluids and immediately swell. This results in polymer fraction reduction (i.e., increasing water content) and alteration of fracture properties [14]. Previous studies on hydrogel swelling have focused on single network hydrogels and bulk properties [15-17]. The correlation between swelling and fracture properties of tough adhesive hydrogels is still unexplored. Thus, to develop tissue adhesives meeting the use inside the body, it is necessary to investigate fracture behaviors of tough adhesive hydrogels, including bulk and adhesion performance, in response to swelling process.

In this thesis, the overall goal is to investigate fracture behaviors of tough adhesive hydrogels. We seek to understand the mechanisms underlying fracture behaviors under cyclic loading and in swelling process. This work is expected to advance the understanding on hydrogel fracture. Also, these findings might be conducive to the development of next-generation tissue adhesives.

1.2. Thesis Structure

This thesis includes six chapters as follows. Chapter 1 introduces the background of the study and thesis structure. Chapter 2 provides a literature review on tough hydrogels, tough hydrogel adhesion, recent progress in fatigue fracture of hydrogels, and the coupling of swelling and fracture of hydrogels. Chapter 3 describes the work done on interfacial fatigue fracture behaviors of tough adhesive hydrogels under cyclic loading based on modified lap-shear tests and theoretical

interpretation. Chapter 4 presents the evolvement of fracture properties of tough adhesive hydrogels during the swelling process, analyzed by Brown's model and finite element simulation. Chapter 5 provides the conclusion of this thesis along with recommendations for future work in this research area.

Chapter 2. Literature Review

2.1. Tough Hydrogels

Section 2.1 reviews tough hydrogels and mechanisms behind their superior mechanical properties, in addition to their promising applications.

2.1.1. Introduction

As an important class of biomaterials, hydrogels consist of a three-dimensional polymer network with crosslinked hydrophilic chains. Due to the high water content, hydrogels have been utilized in a broad range of biomedical applications such as tissue engineering scaffolds [18, 19], carriers for drug delivery [20, 21], tissue adhesives [22, 23], biological models [24, 25] and contact lenses [26]. Furthermore, potential applications of hydrogels have tremendously expanded from clinical use to engineering devices including sensors [27, 28], soft robotics [29, 30] and electronic components [31, 32]. By controlling the synthesis process and compositions, researchers can tune the properties and functions of hydrogels to meet practical requirements.

Despite their outstanding characteristics such as biocompatibility, biodegradability and responsiveness to external stimulations, conventional hydrogels are mechanically weak (elastic modulus $\approx$ 10 kPa and toughness < 10 Jm^{-2}) [33], which dramatically limits their use in load-bearing situations. Especially, given that biological tissues usually exhibit high stiffness, high strength and high toughness, such as cartilage (toughness > 1000 Jm^{-2}) [34] and tendon (strength > 50 MPa) [35], intensive efforts have been made to develop hydrogels with enhanced mechanical properties [36-38].

The poor mechanical properties of conventional hydrogels can be attributed to three factors, including 1) structure inhomogeneity resulting from irregular aggregation of crosslinking points and dispersity of polymer chain lengths [39]; 2) high water content [40]; 3) lack of energy dissipation mechanism [41]. Recently,

many strategies have been proposed to improve mechanical properties of hydrogels, for instance, ionic interactions [42], double networks [37] and fiber-reinforced composite [43]. Briefly, these strategies are aimed to: 1) form ideal polymer networks with homogeneous structure; 2) enhance energy dissipating capability; 3) leverage high-functionality crosslinkers. Examples of tough hydrogels fabricated by these approaches will be described in the next section.

2.1.2. Tough Hydrogels with Reinforced Mechanical Properties

Ideal Polymer Networks

Tetra-poly(ethylene)glycol (Tetra-PEG) Hydrogels

To make homogeneous hydrogels with uniform chain length, Sakai et al. reported a tetra-PEG hydrogel combining two symmetrical tetrahedron-like macromonomers of equal sizes [44]. The obtained networks were found to be extremely uniform with negligible topological defects such as entanglements and loops [45]. Due to the extremely homogeneous 3D tetrahedral structures, these hydrogels exhibit high mechanical strength comparable to cartilage (compressive strength of 2.5 MPa and compression modulus of 40 kPa). It should be noted that, in this method, symmetrical macromers are necessary to fabricate homogeneous hydrogels, thus limiting the available range of polymers.

Networks with Energy Dissipating System

Double network (DN) Hydrogels

Pioneered by Jianping Gong in 2003, double network (DN) hydrogels consist of two interpenetrating polymer networks: the first network is stiff and brittle; the second network is soft and ductile; showing remarkable mechanical properties [37]. DN hydrogels with 90% water content exhibit elastic modulus of 0.1-1.0 MPa, tensile strength of 1-10 MPa, failure strain of 1000%-2000% and toughness of 1000 Jm^{-2} [46]. According to theories proposed by Tanaka et al. [47], upon loading, the first brittle network breaks and microcracks appear, forming a process zone around the crack tip and responsible for energy dissipation. At the same time, the

second ductile network prevents the propagation of microcracks and sustains large deformation, thereby maintaining the integrity of hydrogels. Notably, the concept of double network is general and not limited to certain combinations of polymer pairs.

Alginate/PAAm Tough Hydrogels

Zhigang Suo and coworkers reported a highly stretchable hydrogel made of covalently crosslinked polyacrylamide (PAAm) and ionically crosslinked alginate [38]. This hybrid hydrogel can be stretched 20 times of initial length and achieve tensile strength of 156 kPa and toughness of 9000 Jm^{-2}. During deformation, ionic crosslinks in the alginate network are unzipped, thereby dissipating energy while the PAAm network retains structure integrity, which is credited for its relatively high fracture toughness. After unloading, ionic bonds between alginate and Ca^{2+} crosslinker can be reformed, allowing for the recovery of mechanical properties, which can never be achieved in DN hydrogels. Also, alginate/PAAm hydrogels show excellent biocompatibility, since the implantation of these hydrogels induces a minimal inflammatory response in rats after 8-week implantation [48]. Based on the same method, a series of tough hydrogels with dual crosslinks have been reported, such as PAA/PVA-H_2SO_4 [49], PAM/agar-Li^+ [50] and CCP/MCP-Zn^{2+} [51].

Networks with High-Functionality Cross-Links

Nanocomposite Tough Hydrogels

Another approach is to incorporate nanostructures into hydrogel network. One example is that water-swellable silicate nanoplatelets are introduced to make nanocomposite (NC) hydrogels with excellent mechanical properties [52]. The clay nanosheets absorb polymer chains through ionic and coordination interactions, acting as multifunctional crosslinkers. Since multiple polymer chains can attach to a single clay nanosheet, every individual chain must be disconnected from clay sheets to let crack propagation happen, thus imparting NC hydrogels with high toughness. For example, NC hydrogels composed of poly(N-isopropylacrylamide)

(PNIPAm) polymer network and hectrite clays demonstrate high stretchability (maximum strain larger than 1000%) and can withstand 90% compression, proving their robustness [53].

2.1.3. Applications of Tough Hydrogels

Thanks to the excellence properties of tough hydrogels, they have been proposed and developed for a variety of applications, which are introduced briefly below.

Biosensor

Zhang et al. developed a PVA/Mxene hydrogel used as soft strain sensor with high gauge factor (Figure 2.1) [54]. The hydrogel had a gauge factor of 25 at 40% strain. Because MXene nanosheets worked as multi-functionality crosslinkers, the strain sensitivity and mechanical properties of hydrogels were much improved.

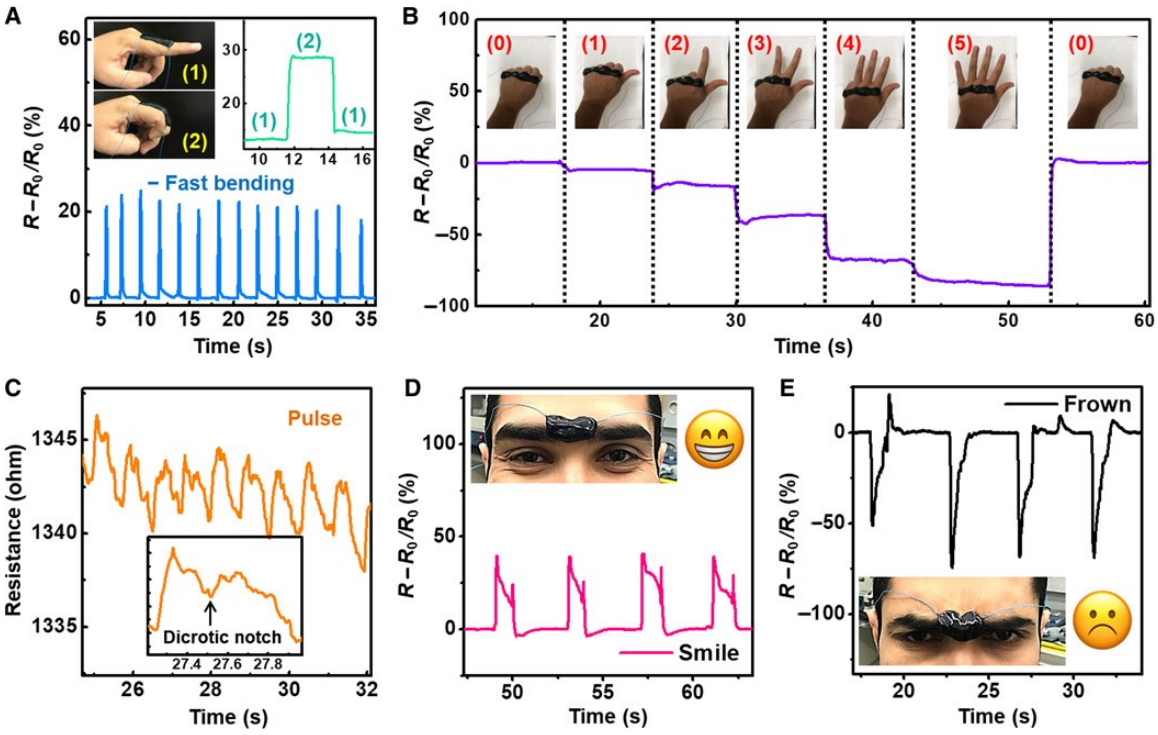

Figure 2.1 (a-e) Resistance changes of PVA/Mxene hydrogel in response to different actions and expressions. (Reproduced from [54], copyright 2018, AAAS).

Soft Actuators

Because hydrogels are able to swell/shrink in response to environmental stimulus, hydrogel-based soft actuators tremendously expand applications of robotics. Yuk et al. developed a bilayer actuator constructed by alginate/PAAm tough hydrogel which could be actuated by hydraulic pressure (Figure 2.2) [29]. Compared to other hydrogel actuators relying on swelling/deswelling driven by osmotic pressure, the responsive time of this hydraulic actuator is much shorter, leading to the development of soft robotics in aqueous environments.

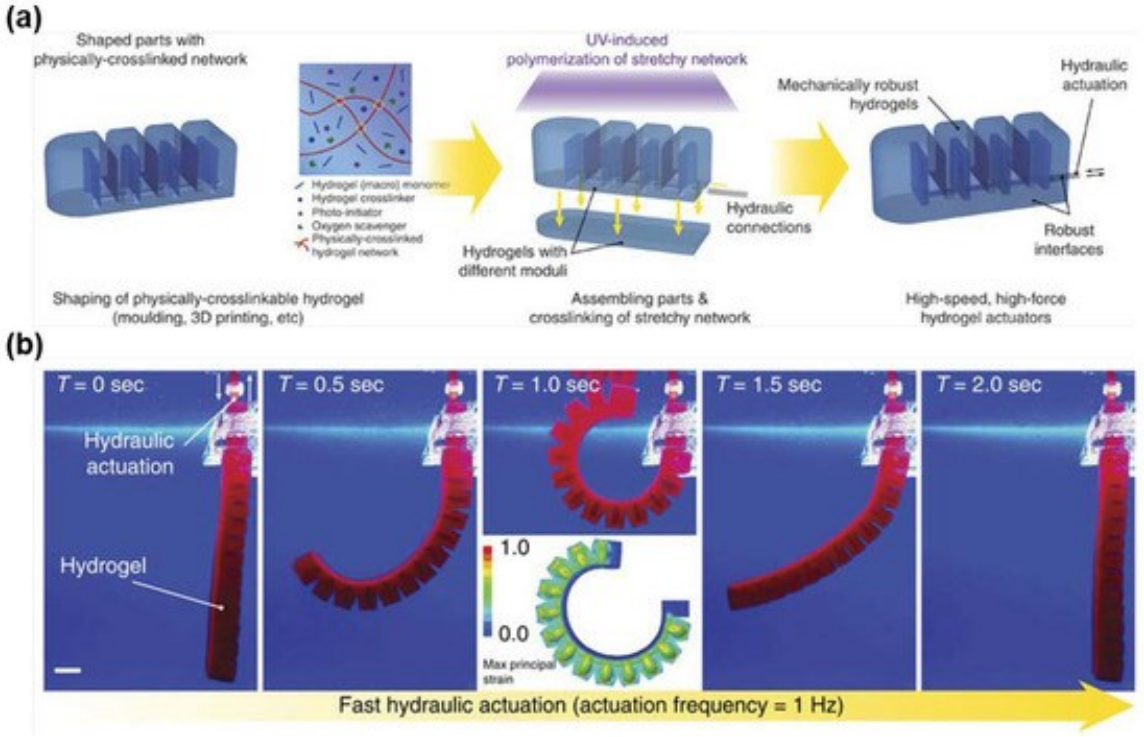

Figure 2.2 (a) Schematic illustration of the structure of hydraulic hydrogel actuator. (b) Fast actuation of hydraulic hydrogel actuator driven by hydraulic pressure. (Reproduced from [29], copyright 2017, Springer Nature).

Drug Delivery

Tough hydrogels have been intensively studied for controlled drug delivery. In 2018, Li et al. formulated an alginate-clay nanocomposite hydrogel to deliver IGF1 mimetic protein (Figure 2.3) [55]. This hydrogel is ideal for drug delivery with its biocompatibility and responsiveness to pH. At a neural pH, proteins are absorbed

to the surface of clay nanoparticles. While at low pH due to injured tissue, hydrogel matrix degrades, and drugs are released.

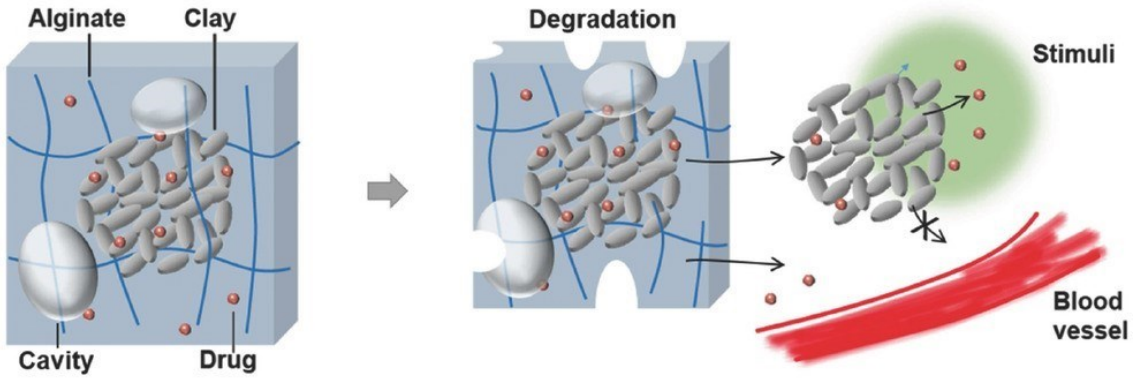

Figure 2.3 Composite hydrogel loads and releases IGF1 proteins. Gray disks: clay nanoparticles; red spheres: adsorbed and free drug molecules; gray bubbles: micro-sized cavities. (Reproduced from [55], copyright 2018, Wiley-VCH).

2.2. Tough Adhesion of Hydrogels

Section 2.2 reviews several methods for achieving tough adhesion of hydrogels with different materials, followed by their potential applications in engineering and medicine.

2.2.1. Introduction

Adhesion research has a long history, which can trace back to the ancient civilization. Hydrogel adhesion refers to forming adhesion between one hydrogel and the other material such as another hydrogel, tissue, glass, metal or any other materials. Achieving strong hydrogel adhesion is critical in a range of applications including wound dressing [56], drug delivery [57, 58], artificial skins [59], tissue repair [60] and bioelectronics [61].

However, achieving effective hydrogel adhesion has been a long-lasting challenge. This is because the majority component of hydrogel is water molecule which does not participate in binding processes or transmit force, thereby preventing adhesion. Traditional adhesives, such as cyanoacrylate, is cytotoxic and only works for dry

surfaces, since it solidifies instantaneously in contacting with water [62]. Thus, it is an urgent need to develop a new way for wet adhesion.

Recently, a series of methods have achieved strong and tough hydrogel adhesion on diverse substrates, including metals, glass, polymers and tissues, by combining chemistry, topology and mechanics [4, 5, 63-65]. In general, the design principle of tough hydrogel adhesion is to first form strong linkages at the interface, such as covalent bonds [66], non-covalent links [67], bridging polymers [4] and nanoparticles [68]. Then the hydrogel matrix must be tough enough to dissipate energy during detachment. The total adhesion energy is a sum of intrinsic adhesion energy dominated by interfacial linkages and the energy dissipation inside hydrogel matrix. The synergy of these two mechanisms yields high adhesion energy, unseen with conventional hydrogel adhesives.

2.2.2. Strategies for Tough Hydrogel Adhesion

Covalent Bonding

Covalent bonds have been widely used to create adhesion between hydrogels and various materials, including carbon-carbon [69], carbon-nitrogen [4], silicon-oxygen [70] and carbon-sulfur [71] bonds. Yuk et al. first achieved strong hydrogel adhesion by anchoring polymer chains of alginate-PAAm hydrogel on substrates [5]. In this case, substrate surfaces are first modified by silanes to add methacrylate groups. After casting the precursor, the surface-modified substrates are covalently grafted to alginate-PAAm hydrogel network via in situ polymerization during cure. Due to the superior fracture properties of alginate-PAAm hydrogel, a significant amount of energy is dissipated during detachment, thus achieving high adhesion energy from 1000 Jm^{-2} to 1500 Jm^{-2} on metals, glass, silicon and ceramics. Notably, this method is not limited to alginate-PAAm hydrogel, and it is expected to work for any hydrogel synthesized by free radical polymerization.

Bridging Polymers

Since it involves toxic chemicals, the above covalent bonding method is not applicable to tissue adhesion. Recently, Li et al. successfully employed bridging polymers to bond alginate-PAAm hydrogels and tissues [4]. A species of polymers containing primary amine group can be adopted as bridging polymers, such as chitosan, polyallylamine and polyethylenimine. When an aqueous solution of bridging polymers mixed with 1-ethyl-3-(3- dimethylaminopropyl)carbodiimide (EDC) and N-hydroxysulfosuccinimide (NHS) is cast between hydrogel and tissue, the NH_2 groups on the bridging polymer and the -COOH groups on the tissue and alginate form amide bonds through EDC chemistry. Meanwhile, the bridging polymer interpenetrates into hydrogel and tissue, forming a network as a topological stich. This method synergizes interfacial bridging and energy dissipation of tough hydrogels, achieving an adhesion energy over 1000 Jm^{-2} on various tissues including skin, heart and liver, even in the presence of blood.

Physical Crosslinks

Various physical crosslinks such as crystalline domains [67], glassy staples [72] and hydrogen bonds [73] can be adopted to achieve strong hydrogel adhesion. Because each physical crosslink can connect multiple polymer chains, intrinsic adhesion energy is largely enhanced. For example, Liu et al. implemented nanocrystalline domains to adhere PVA hydrogels on diverse engineering materials [67]. First, PVA hydrogels are synthesized on cleaned substrates. After dry-annealing treatment, PVA hydrogels form nanocrystalline domains which strongly bond to substrates via high-density hydrogen bonds. Because it requires much higher energy to fracture nanocrystalline domains at the interface than polymer chains, this method can even achieve higher adhesion energy (7500 Jm^{-2}) than tough alginate-PAAm hydrogel adhesion (1500 Jm^{-2}). In addition, it shows excellent fatigue-resistant adhesion with an interfacial fatigue threshold of 800 Jm^{-2}, comparable to the adhesion of tendons, ligaments and cartilages [34, 74, 75]. However, this method is limited to the specific material system and by the lengthy processing steps.

Mechanical Interlocking

To apply the concept of mechanical interlocking in hydrogel adhesion, Cha's group designed a microneedle patch inspired by sandbag worms [76]. The microneedle patch contains a mussel adhesive protein-based sticky shell for adhesion and a silk fibroin-based rigid core for fixation. After piercing into soft tissues, the outer microneedle shell swells and forms mechanical interlocking with surrounding tissue. The microneedle patch could achieve a high adhesion strength (~ 190 kPa) on wet and dynamic tissue. More interestingly, microneedle tips could be loaded with drugs to provide controlled drug delivery in a minimally invasive way.

2.2.3. Applications of Hydrogel Adhesion

With strong hydrogel adhesion achieved, researchers have been exploring its application in various settings, summarized below.

Stretchable Circuits

Yuk et al. developed a conductive hydrogel adhesive that can bond two electrodes (Figure 2.4) [5]. The circuit made of electrodes and hydrogel enables powering a LED light under stretching. Further, the conductivity of hydrogel-electrodes circuit is not affected even after undergoing 1000 loading cycles. This hydrogel adhesive promotes the development of soft electronics.

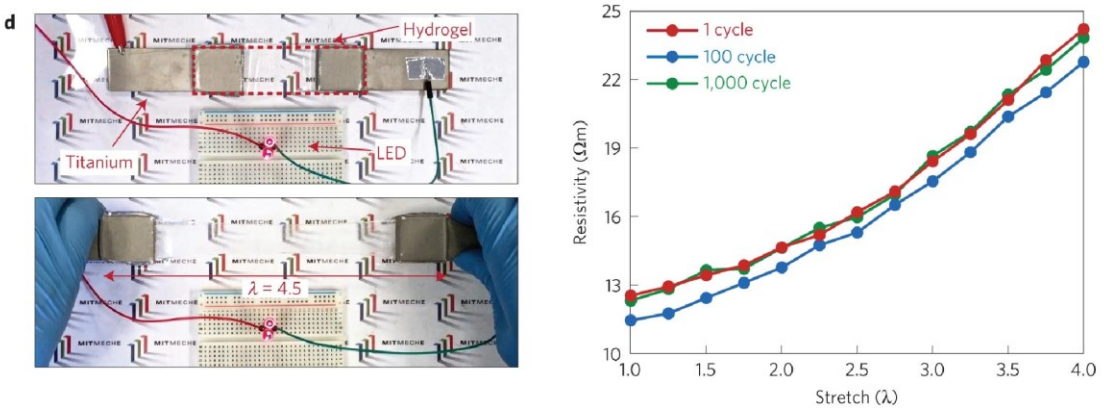

Figure 2.4 Stretchable circuit based on the adhesion of tough hydrogels. (left) The circuit is conductive to power a LED light under a stretch of 4.5 times. (right) The conductivity of the circuit is not affected after undergoing 1000 loading cycles. (Reproduced from [5], copyright 2015, Springer Nature)

Tissue Adhesives

Zhao's group invented a hydrogel adhesive that can adhere to various tissues in less than 5 seconds (Figure 2.5) [56]. Due to its self-adhesive ability, the hydrogel adhesive can be easily used for wound dressing, drug delivery and adhering biosensors without preparing additional glues.

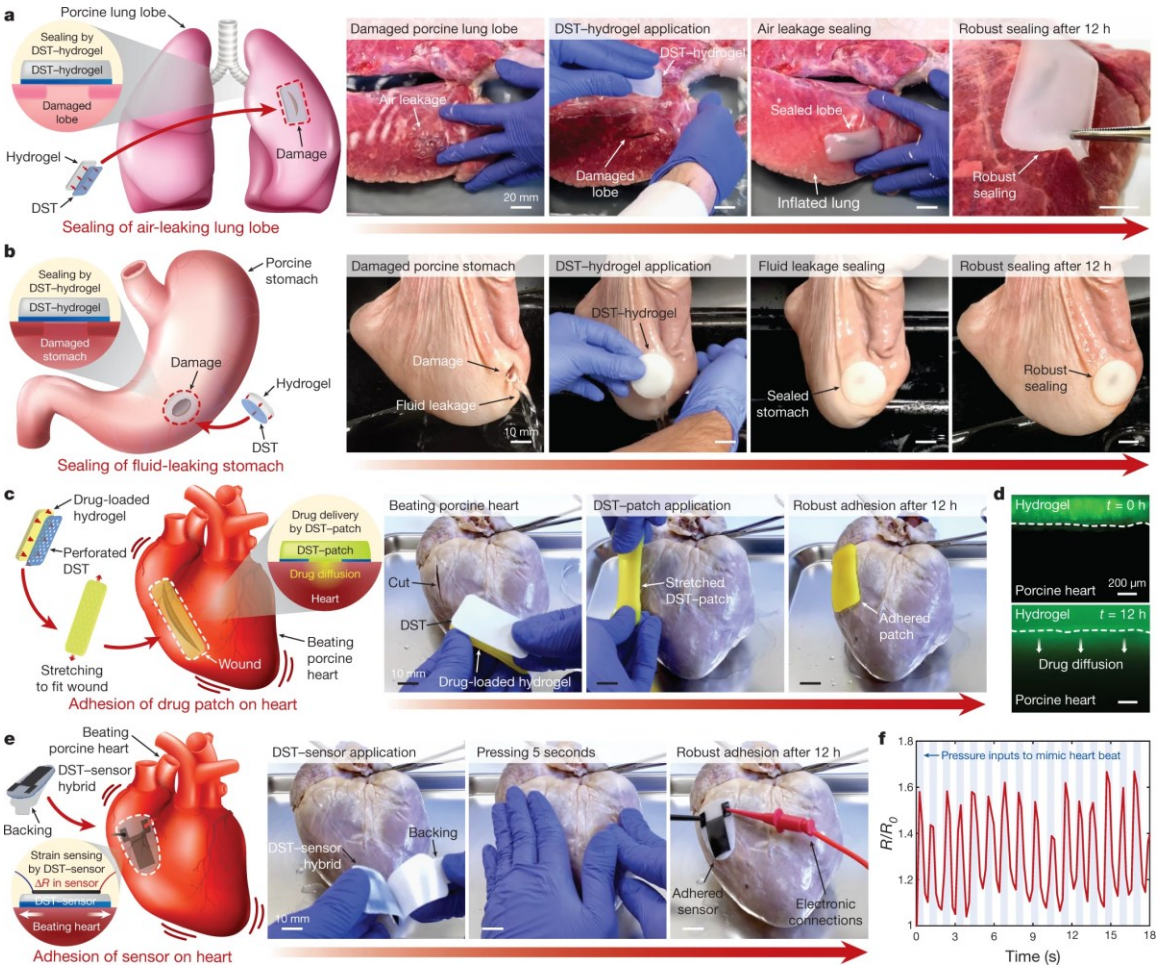

Figure 2.5 Potential applications of double-sided tape hydrogel. (a) Sealing of an air-leaking porcine lung. (b) Sealing of a fluid-leaking porcine stomach. (c) A drug-loaded patch on a porcine heart. (d) Diffusion of drug into heart tissue. (e) Adhering a strain sensor on a porcine heart. (f) Normalized electrical resistance of the strain sensor. (Reproduced from [56], copyright 2019, Springer Nature)

Drug Delivery

Hydrogels capable of adhering to the skin can be used for transdermal drug delivery. For example, Jung et al. proposed a polyacrylamide/polydopamine

hydrogel embedded with mesoporous silica nanoparticles (MSNs) as a transdermal drug delivery patch (Figure 2.6) [58]. The incorporation of MSNs not only enhances the cohesion of hydrogel patch, but also further increases the adhesiveness. With drugs laden in MSNs, this hydrogel patch demonstrates a simple but effective transdermal drug delivery system.

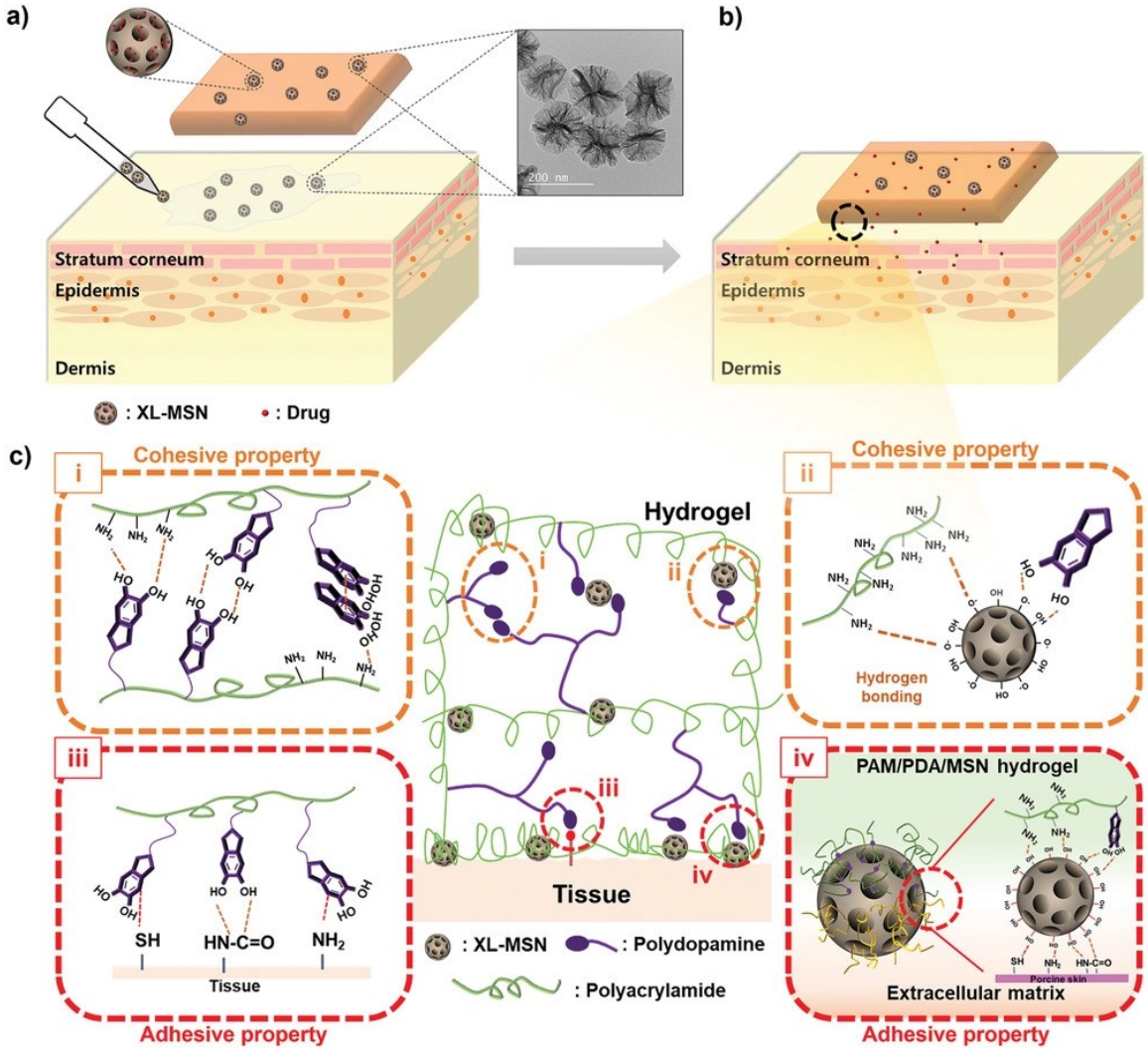

Figure 2.6 (a, b) Schematic illustration of adhesive hydrogel patch for transdermal drug delivery. (c) Interactions among nanoparticles, polymer chains and tissues. (Reproduced from [58], copyright 2020, Wiley-VCH)

2.3. Fracture Behaviors of Hydrogels

Section 2.3 first reviews experimental methods for measuring cohesion energy (i.e., toughness) and adhesion energy of hydrogels. This is followed by a brief summary

of fatigue fracture of hydrogels. The effect of swelling on fracture properties of hydrogels is discussed in the end.

2.3.1. Experimental Measurement of Fracture Properties

Cohesion Energy

Cohesion energy (i.e., toughness) characterizes the resistance of materials to crack growth. The critical energy release rate G during crack propagation is often used to calculate cohesion energy. When the energy release rate G at the crack tip determined by external loading reaches cohesion energy, the crack starts to grow.

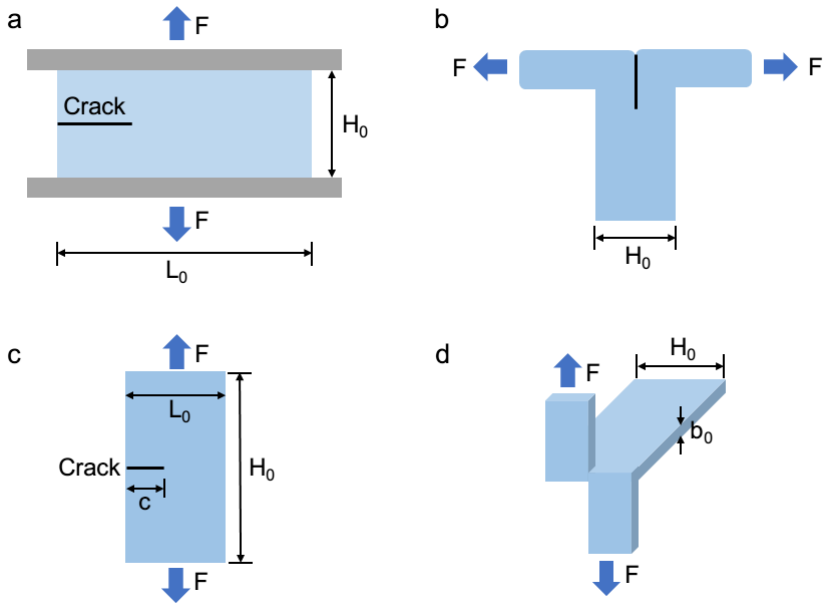

Figure 2.7 Test configurations for measuring cohesion energy. (a) Pure shear test. (b) Simple extension test. (c) Single edge crack test. (d) Tearing test.

Pure shear test

Pure shear test proposed by Rivlin and Thomas is extensively adopted to measure the toughness of soft materials, such as rubbers and hydrogels [77-79]. In the pure shear test, the sample geometry is a long thin strip. In other words, width, height and thickness are L_0, H_0 and b_0, satisfying $L_0 >> H_0 > b_0$ (Figure 2.7a). The sample is pre-cut with a long edge crack before loading. When the sample is stretched vertically, the energy release rate is calculated by [77]:

$$G = W(\lambda)H_0 \quad (1)$$

where W is the strain energy density given by the area under the stress-stretch curve when stretching an uncracked sample of the same geometry. λ is the stretch imposed to the pre-cut sample.

Simple extension test

In simple extension test, the sample geometry is similar to that in pure shear test. The sample has a length of L_0, a height of H_0 and a thickness of b_0. Upon loading, two arms at the cracked end are stretched and peeled apart as shown in the Figure 2.7b. The energy release rate G is written as [77]:

$$G = \frac{2\lambda F}{b_0} - WH_0 \quad (2)$$

where F is the force applied to the arms, λ and W are the stretch and strain energy density of the arms. When the deformation of the arms is restricted or neglected, the equation (2) is reduced to $G = \frac{2F}{b_0}$. Notably, if the deformation in arms is large, the strain energy density W and the stretch λ cannot be neglected.

Single edge crack test

Single edge crack test was initially used by Greensmith [80] to measure the toughness of vulcanized natural rubbers. If the sample geometry meets the requirement $c \ll L_0 \ll H_0$ (Figure 2.7c), the energy release rate is approximately given by [80]:

$$G = \frac{6}{\sqrt{\lambda}} W(\lambda)c \quad (3)$$

where W is the strain energy density of an uncracked sample under uniaxial tension.

Tearing test

Tearing test, also known as trouser-tear test, has been used to measure the fracture of rubber [81], elastomers [82] and tough hydrogels [83]. In the tearing test, two arms are stretched to the opposite direction by an out-of-plane loading (Figure

2.7d), named as Mode III failure. However, from the energetic view, the energy release rate G is the same as that in simple extension test. If the deformation of arms is neglected, the equation (2) can be reduced to $G = \frac{2F}{b_0}$.

Adhesion Energy

Adhesion energy is defined as the energy required for a crack to grow per unit area at interface. To characterize the quality of adhesion, three types of mechanical tests (i.e., probe pull, lap shear and peel) are usually adopted. Typically, the probe pull and lap shear tests are used to measure adhesion strength (Figure 2.8a&b), and the peel test is used for adhesion energy (Figure 2.8c&d). However, recent studies showed lap shear could also be used to measure adhesion energy of hydrogels [84-86]. It is worth noting that adhesion strength and adhesion energy are two independent properties.

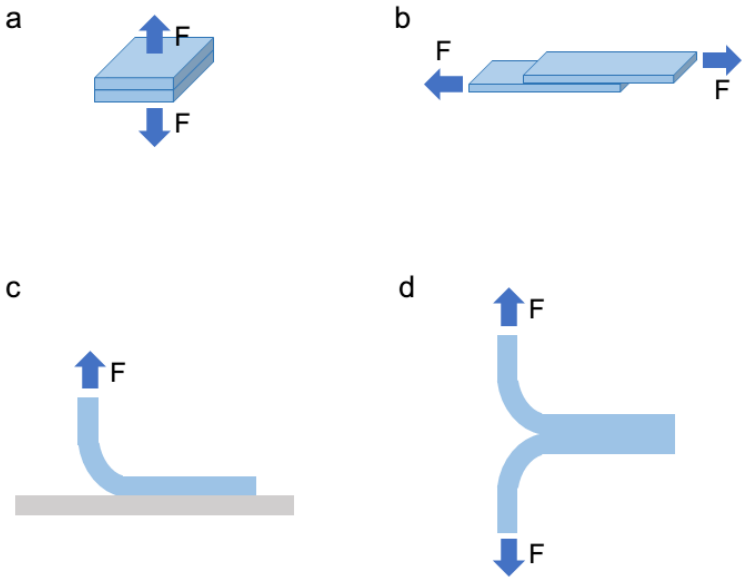

Figure 2.8 Test configurations for measuring adhesion. (a) Probe pull test. (b) Lap shear test. (c) 90° peel test. (d) 180° peel test.

Lap shear test

In the lap shear test, two adherends are bonded together by a thin layer of adhesive (Figure 2.8b). The overlap area is called lap shear joint. When the applied force is parallel to adherends, a crack initiates and propagates along the interface,

simulating a common failure of adhesive joint. In this case, the energy release rate is the difference between the elastic energy per unit length of two adherends [87]:

$$G = \frac{b_0}{4E}\left(\frac{F}{wb_0}\right)^2 \quad (4)$$

Where b_0, E, w are the thickness, elastic modulus and width of adherends, respectively.

Peel test

Peel test is typically carried out at a constant peel velocity or under a constant load. Peel angle is usually fixed at 90° (Figure 2.8c) or 180° (Figure 2.8d) for simplicity [88]. The advantage of peel test is that in a steady crack propagation state at a constant peel velocity, the applied peel force directly translates into the interfacial fracture energy, i.e., adhesion energy. Two adherends are usually glued with stiff backings to restrict the deformation of two arms during peel tests. In 90° peel test, the adhesion energy is given by:

$$G = \frac{F}{w} \quad (5)$$

Where w is the width of the adherends. In 180° peel test, namely T-peel test, the equation becomes $G = \frac{2F}{w}$.

2.3.2. Fatigue Fracture of Hydrogels

Fatigue fracture has been extensively studied in engineering materials, such as metals, plastics, ceramics and composite materials [89-92]. Only recently, several papers reported the fatigue fracture of hydrogels [11-13, 93-96]. Fatigue fracture refers to the crack grows under cyclic loading, eventually leading to the fracture of sample. And fatigue threshold is defined as a critical load below which the crack does not grow no matter how long the cyclic loading is applied. Here, we summarize representative data of fatigue of hydrogels.

Polyacrylamide (PAAm) Hydrogels

Tang et al. first reported delayed fracture and cyclic fatigue fracture of PAAm hydrogels [13]. The toughness of the PAAm hydrogel synthesized from 2.2 M monomer and 0.156% crosslinker is reported to be 56.8 $\pm$ 3.8 Jm^{-2}. For a pre-cut PAAm hydrogel under static loading, delayed fracture happens when the energy release rate is between the fracture toughness and the threshold for delayed fracture which is reported to be 35.4 Jm^{-2}. For a pre-cut PAAm hydrogel under cyclic loading, fatigue failure is observed when the energy release rate is higher than the cyclic-fatigue threshold measured at 7.03 Jm^{-2}. According to the Lake-Thomas model [97], the crack would gradually extend by cutting polymer chains ahead of the crack when the applied load is above the fatigue threshold, which indicates the fatigue threshold increases with polymer fraction and polymer chain length [94]. Zhang et al. further studied fatigue fracture of PAAm hydrogels with different water contents and confirmed that the fatigue threshold increases with the polymer fraction [94].

Double-network (DN) Hydrogels

Gong et al. reported the first double-network hydrogel with high toughness (~4000 Jm^{-2}) [37]. The DN hydrogel consists of a soft PAAm network and a stiff PAMPS network. Zhang et al. studied the fatigue fracture of DN hydrogel under cyclic loading and found that DN hydrogel has a high fatigue threshold over 400 Jm^{-2} [96]. Because PAMPS network is covalently connected, the fatigue damage in DN hydrogel is completely irreversible, which means DN hydrogel would severely suffer from cyclic loading.

Alginate-PAAm Hydrogels

Sun et al. invented an alginate-PAAm hydrogel whose toughness is above 8000 Jm^{-2} [38]. In alginate-PAAm hydrogel, PAAm forms a covalently crosslinked network providing elasticity and alginate forms an ironically crosslinked network dissipating energy. Sun et al. also found that alginate-PAAm hydrogel could heal from fatigue damage by heating the hydrogel, since Ca^{2+}-alginate bonds could recover at elevated temperature [12, 38]. The self-recovery property of the

hydrogel might affect its fatigue behavior. So, Bai et al. investigated fatigue fracture of alginate-PAAm hydrogel under cyclic loading [12]. At a fixed cyclic stretch, the crack growth speed is fast at beginning, but gradually reaches a steady state. The fatigue threshold of alginate-PAAm hydrogel is reported to be 53 Jm^{-2}.

PVA-PAAm Hydrogels

Bai et al. also studied fatigue fracture of PVA-PAAm hydrogels [11]. PVA chains could form hydrogen bonds with themselves and with PAAm networks. Under loading, hydrogen bonds break, imparting hydrogel energy dissipation capability. They found that a PVA-PAAm hydrogel without precut is free from fatigue damage, as hydrogen bonds reform in unloading stage and the hydrogel recovers. However, cyclic fatigue fracture is observed in a PVA-PAAm hydrogel with a precut. The fatigue threshold of PVA-PAAm hydrogel is measured to be 9.5 Jm^{-2}, similar to that of PAAm hydrogel [13], proving that the fatigue threshold mainly depends on covalent network.

2.3.3. Effects of Swelling on Fracture Properties of Hydrogels

Swelling behaviors of hydrogels have been extensively studied [98]. Various models based on kinetics and thermodynamics of swelling have been proposed [99-101]. Among them, the most well-known model connecting swelling and mechanics is Flory–Rehner (F-R) model [102]. Assuming the free energy of network is the summation of that of individual chains and all chains follow Gaussian distribution [103], F-R model successfully describes the relationship between microscopic molecular structure and macroscopic elastic properties. For example, according to F-R model, the elastic modulus E has a scaling with respect to polymer fraction, i.e., $E \sim \phi^{1/3}$ [104].

Even though many models built on scaling theory capture the elastic response of hydrogels in swelling, few studies pay attention to fracture properties. Chen et al. compared toughness of agar-PAAm hydrogels in as-prepared state and swollen state [105]. Typically, swelling weakens mechanical properties. But Chen et al. found that the effect of swelling could be minimized by increasing agar

concentration, achieving similar toughness in as-prepared state (3988 Jm^{-2}) and swollen state (3960 Jm^{-2}). Chen's study demonstrates high toughness could be obtained in both as-prepared state and swollen state, broadening applications of hydrogels in aqueous environment.

Kundu et al. quantitatively investigated the effect of swelling on elasticity and toughness of PAAm hydrogels [106]. By using a simple experiment, cavitation rheology, Kundu et al. measured elastic modulus E and fracture toughness G_c of hydrogels with various polymer fractions ϕ. The results show that the elastic modulus E and toughness G_c have a scaling relationship with polymer fraction φ, i.e., $E \sim \phi^{2.3}$ and $G_c \sim \phi^{5/24}$. A scaling theory is adopted to capture the transition from elastic deformation to fracture.

Even though F-R model is widely used to interpret the elastic response of swollen hydrogels, Li et al. points out that the scaling exponent is not all the same, which cannot be explained by F-R model [107]. By measuring elastic modulus of PAAm hydrogels in swollen state and dehydrated state separately, Li et al. discovered that the scaling laws are different in two states [107]. A scaling theory is proposed and successfully explains the discrepancy. Furthermore, Li et al. proposed a theoretical model expressing the fracture threshold as a function of polymer fraction and found that the fracture threshold obeys the same scaling law as elastic modulus. A connection between elastic modulus and fracture threshold is established.

Chapter 3. Article 1: Interfacial Fatigue Fracture of Tissue Adhesive Hydrogels

Xiang Ni[1], Chao Chen[2], Jianyu Li[1,3*]

1 Department of Mechanical Engineering, McGill University, Montreal, QC H3A 0C3, Canada

2 Department of Polymer Science and Engineering, University of Massachusetts Amherst, Amherst, MA 01003, USA

3 Department of Biomedical Engineering, McGill University, Montreal, QC H3A 0C3, Canada

* Corresponding author. Email: jianyu.li@mcgill.ca

Abstract

Tissue adhesive hydrogels find increasing use in the clinic, but their response to prolonged cyclic deformation remains unexplored. The lack of understanding hinders the development and application of tissue adhesive hydrogels, particularly in the applications interfacing with repeatedly deforming tissues such as heart and lung. Here we study the interfacial fatigue fracture of a tissue adhesive hydrogel based on tough hydrogel, called tough adhesive (TA), using a fracture mechanics approach. We perform modified lap-shear tests with three types of loading (e.g., monotonic, static, and cyclic loads). We observe shakedown of the load-displacement curves during cycling and two interfacial fracture phenomena: fast debonding and interfacial fatigue fracture. We confirm the existence of a fatigue threshold (24.4 J m^{-2}) for the TA-skin interface, below which the interface is immune against prolonged cyclic deformation. The threshold is lower than the adhesion energy (580 J m^{-2}) for fast debonding. We also compare the interfacial fatigue fracture with the fatigue of bulk hydrogels. This work will promote further mechanistic investigation on interfacial fatigue fracture and the development of fatigue-resistant tissue adhesives.

Keywords: tissue adhesives, hydrogels, fatigue, adhesion, crack growth

3.1. Introduction

Tissue adhesive hydrogels stick to biological tissues and close wounds. They have been deemed to be promising reinforcements and replacements for sutures and staples [1,2]. Examples of clinically used tissue adhesive hydrogels include Coseal® (Baxter), BioGlue® (CryoLife), TISSEEL® (Baxter) and Evicel®(Ethicon). They find increasing use in many branches of medicine, including tissue repair [3–5], surgical sealants [6–8], drug delivery [9,10], device fixation [11], and wound dressings [12]. However, the performance of tissue adhesive hydrogels remains unsatisfactory due to their limited mechanical properties. They are often vulnerable to rupture or debonding from tissues especially under mechanically demanding tissue environments [3]. To overcome the limitations, new tissue adhesive hydrogels based on tough hydrogels, called tough adhesive (TA), are developed recently, which combine superior toughness and tissue adhesive properties [3]. There are other tissue adhesives with enhanced mechanical performance, including thermalresponsive adhesives [12], mussel-inspired adhesives [13], photo-controllable adhesives [14] and degradable adhesives [15]. They are promising to expand the application scope of tissue adhesive hydrogels to the areas involving mechanically dynamic tissues such as heart, tendon, and cartilage. Preclinical studies suggest that the improvement of mechanical properties of tissue adhesives can help mitigate surgical complications and promote wound healing, for instance, in skin wound management [12] and tendon repair [16].

Cyclic deformation is ubiquitous in the human body, for instance, a heart beats for 2.5 to 3 billion times [17] and a lung gets inflated and deflated for 500 to 800 million times [18] in one's life. To interface such tissues with tissue adhesive hydrogels, one must study the interfacial fatigue fracture of tissue adhesive hydrogels, i.e., how they respond to the prolonged cyclic deformation. Previous studies on tissue adhesive hydrogels focus on either monotonic loading or basic characterization under cyclic deformation without examining crack extension behavior [3]. Recent

studies report the fatigue fracture of bulk hydrogels, including polyacrylamide hydrogels [19], tough hydrogels [20], double network hydrogels [21] and self-recovering hydrogels [22]. However, the interfacial fatigue fracture of hydrogels, in general, remains largely unexplored till now.

The interfacial fatigue fracture is traditionally studied on engineering materials such as metals [23] ceramics [24], and epoxy [25]. To study the interfacial fatigue fracture of tissue adhesive hydrogels, it is urgent to develop new testing methods. The common testing methods for tissue adhesives focus on the adhesion strength or the failure force under monotonic load. But the fracture processes better relate to the fracture energy or the critical energy release rate [26]. The widely used methods and equipment for measuring fracture energy cannot be directly applied in the interfacial fatigue study of tissue adhesives due to the geometric constraints of biological tissues, the loading control (displacement versus force-controlled) and the dehydration issue. Further development is needed for characterization methods that allow for facile determination and control of the energy release rate over cycles.

Here we will explore the interfacial fatigue fracture of tissue adhesive hydrogels. We will choose the TA as a model tissue adhesive hydrogel, as they demonstrate superior tissue adhesive property and translation capacity [3]. To study the interfacial fracture behavior of TA on porcine skin, we will modify the lap-shear method and test three types of loading: monotonic, static, and cyclic loads. We will characterize the crack extension behavior under different loading, determine the adhesion energy for fast debonding and the threshold, if any, for interfacial fatigue fracture. We will also compare the interfacial fatigue fracture with the fatigue of bulk hydrogels. This study will answer fundamental questions regarding the interfacial fatigue fracture of tissue adhesive hydrogels. For instance, does the tissue adhesion fatigue? What is the interfacial fatigue threshold? It will also provide insights into the development of tissue adhesive hydrogels with high fatigue resistance.

3.2. Experimental section

3.2.1. Materials

Most of the chemical reagents were purchased from Sigma Aldrich, including acrylamide (AAm, monomer), N,N'-methylenebis(acrylamide) (MBAA, crosslinker), N,N,N',N'-tetramethylethylenediamine (TEMED, accelerator), ammonium persulfate (APS, initiator), calcium sulfate, N-hydroxysulfosuccinimide (NHS), and 1-ethyl-3-(3-dimethylaminopropyl)carbodiimide (EDC). Alginate (I-1G) was purchased from KIMICA Corporation. Chitosan (deacetylation degree 95%, medium to high molecular weight) was purchased from Xi'an Lyphar Biotech (Shanxi, China). We purchased acrylic sheets from McMaster-Carr used to make reaction molds. Fresh porcine skin was purchased from a local grocery store.

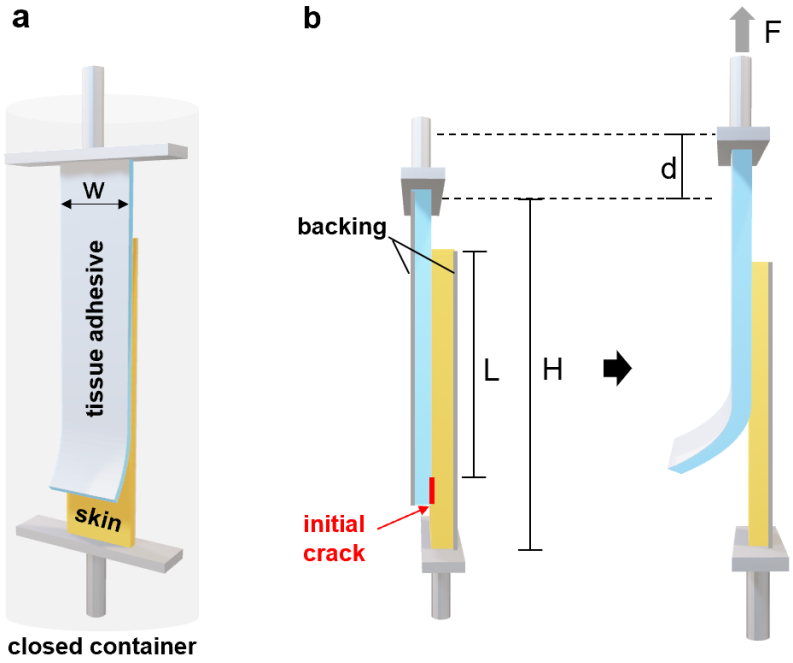

Figure 3.1 Schematics of the specimen and testing method. (a) A modified lap-shear specimen is enclosed inside a closed chamber and stretched unidirectionally. (b) Grips pull the specimen with a force F and a prescribed displacement d. The outer surfaces of the adhesive and the skin are glued to rigid plastic films to concentrate the work at the crack tip. The initial length of the specimen is L and the nominal strain applied onto the adhesive joint is ε=d/L.

3.2.2. Specimen Preparation

The tough adhesive as a model tissue adhesive hydrogel was synthesized with a two-step method following a protocol reported previously [3]. We first synthesized alginate-polyacrylamide tough hydrogels as the adhesive matrix and then activated their surface with chitosan and coupling reagents (i.e., EDC and NHS). Briefly, we dissolved 6.76 g of AAm monomers and 1.128 g of sodium alginate in 50 mL of deionized water. We mixed 20 ml of the AAm-alginate solution with 72 μL of MBAA aqueous solution (0.02 g mL^{-1}) and 16 μL of TEMED within a syringe. Meanwhile, 452 μL of APS solution (0.066 g mL^{-1}) and 382 μL calcium sulfate slurries ($CaSO_4$, 0.207 g mL^{-1}) were drawn into another syringe. Two syringes were mixed with a Luer Lock connector to form a homogeneous solution. The mixture was immediately injected into a 65 × 15 × 1.5 mm^3 acrylic mold covered with a glass plate and kept at room temperature for 24 hours to complete the reaction. We dissolved 1 g of chitosan powder into 50 mL of deionized water with 400 μL of acetic acid added for a final pH of 4.5. The mixture was stirred overnight to form a homogenous solution and kept at 4 ^oC before use.

We cut the fresh porcine skin into slices of area 65 × 15 mm^2. We first mixed 60 mg of EDC and 60 mg of NHS to 1 mL of the chitosan solution. We spread the mixture onto the epidermal surface of the porcine skin and immediately placed the tough hydrogel on top. The length of the overlapping joint was 45mm for adhesion. An initial crack was made with a thin polyethylene terephthalate film (PET, 15 × 5 × 0.1 mm^3) on one edge of the hydrogel using Krazy glue, as illustrated in Figure 3.1. The mold was covered with an acrylic sheet and clamped with binder clips for a gentle compression (Figure 3.6). The whole mold was stored in a zip bag at 4 ^oC overnight. Before testing, we glued PET films on the back of the adhesive and the skin to constrain their deformation. Following the same procedure above, we prepared the TA-hydrogel specimens by replacing the pigskin with another slice of alginate-PAAm hydrogel adhering to TA.

3.2.3. Mechanical testing

To study the interfacial fatigue fracture, we adopted the modified lap-shear method under prescribed displacements of different magnitudes (Figure 3.1a) since the widely used mechanical testing systems (e.g., Instron, MTS) are typically displacement-controlled. This choice of the testing method enables a stable crack extension to aid the crack measurements during the cyclic tests. It is a contrast to the commonly used tests for interfacial fracture (e.g., peeling and tear tests), which are difficult, if not impossible, to maintain the mechanical load at the crack tip using a displacement-controlled testing system given a gradual crack extension. The lap-shear method is widely used to characterize tissue adhesives and the resulting loading condition is relevant to that experienced by the tissue adhesives used in vivo. Both TA and the adherend (either skin or hydrogel) were glued with rigid PET films, to constrain the energy dissipation at the interface and facilitate the determination of energy release rate G over cycles. An Instron machine (model 5965), equipped with a 1 kN load cell and a closed chamber, was used (Figure 3.7). We enclosed the whole specimen in the closed chamber and sprayed deionized water frequently on the inner chamber surface, to maintain high humidity and to prevent dehydration of the adhesive and the skin. We confirmed the mass loss of the adhesive and the tissue was within 5% throughout the tests (Figure 3.11).

The Instron machine stretched the two arms of the specimen unidirectionally with a force F and a prescribed displacement d. Three kinds of loading were tested: monotonic, static and cyclic loads. The displacement rate was fixed at 30 mm min^{-1} for monotonic and static loads. For cyclic loads, the loading frequency is fixed at 1 Hz. As the initial length of the adhesive joint was L and the width w, the applied line load P and the nominal strain ε are F/w and d/L, respectively. The force and displacement were recorded throughout the test and used to plot the load-strain curves. To determine the length of adhesive joint L, a digital camera (AUSDOM AM615) was used to record the crack extension. To facilitate the determination of the crack extension, we attached a ruler liner onto the side of the specimen (Figure

3.7). The energy release rate G is defined as the reduction of the potential energy associated with the crack advancing by a unit area. With known load P and joint length *L*, the G takes the following form:

$$G = t_A W_A + t_T W_T$$

where t is the thickness, W is the strain energy density of the sheared region under a certain load, and subscriptions A and T refer to the adhesive and the tissue, respectively (See Supporting Information). Our measurements showed that the elastic modulus of the skin was >100 times than that of the adhesive, while t_A and t_T are in the same order of magnitude. The elastic moduli of the adhesive matrix and the skin were determined with unidirectional tensile tests (Figure 3.8). Therefore, W_T can be safely neglected and G equaled to $t_A W_A$. In support of this, we observed that the skin deformed minimally in our experiments. In the case of the TA-hydrogel specimen, the hydrogel was identical with that used as the adhesive matrix; the G is calculated by $2 \times t_A W_A$. Given the initial crack much smaller than the adhesive joint, we can approximate G with the area under the shear load-strain curve of the modified lap-shear specimen, i.e., $G = \int P d\varepsilon$. Our tests also validated the approximation by showing similar shear stress-strain curves measured with the modified lap-shear specimen and the simple shear specimen consisting of the adhesive alone (Figure 3.9).

3.3. Results and Discussion

3.3.1. Fast debonding

We first characterize fast fracture of the TA-skin interface under monotonic load (Figure 3.2a and 3.2b). The applied strain increases monotonically until the initial crack extends through the interface and a fast debonding occurs. The critical load P_c and the critical strain ε_c to separate the TA and the skin are recorded (Figure 3.2b). As both the TA and the skin are constrained with rigid PET films, the critical energy release rate for the interfacial fracture, or the adhesion energy, equals to

$t_A W_A(P_c)$. The adhesion energy defines the work required to advance a crack by a unit area at the adhesion interface. The results show the adhesion energy is 580.0±105.8 Jm^{-2}, reconfirming that the TA forms strong adhesion on the skin. The measured adhesion energy is in a reasonable error range considering the variance of biological tissue. It is worth mentioning that the value is lower than that measured with 180-degree peeling tests [3]. It can be attributed to the difference in the testing method (lap-shear versus peeling), and loading conditions (loading rate), which deserves further investigation but isn't pursued here. The critical strain and the adhesion energy inform us of the upper bound of the loading condition for the fatigue study below.

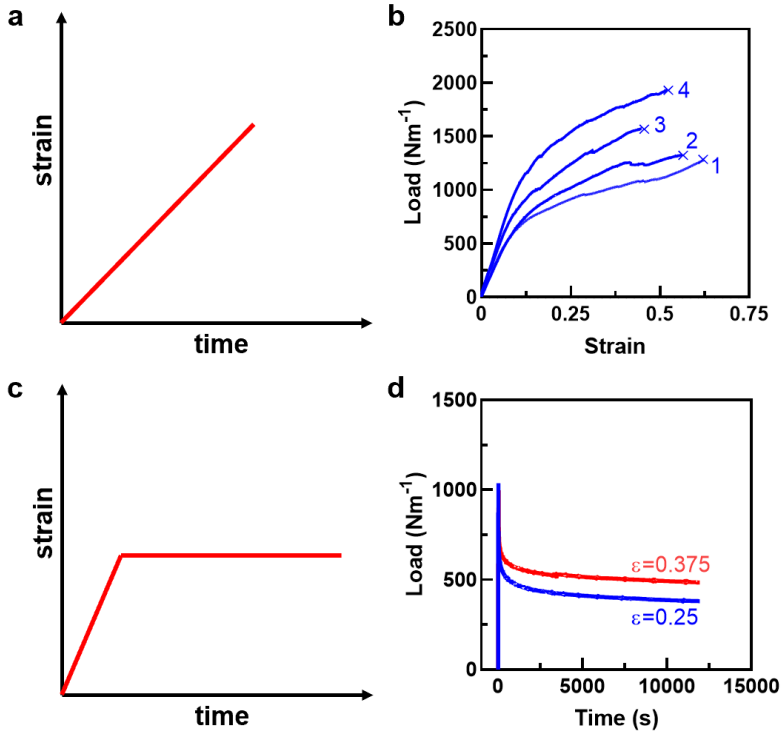

Figure 3.2 Fast and static fatigue tests. (a) Loading profile of monotonic load. (b) Load-strain curves of the four tested specimens. Variation is typical in fracture tests. (c) Loading profile of static load. (d) Load relaxation during static fatigue tests. The applied strains are as labelled.

3.3.2. Static fatigue tests

To examine whether the crack advances under static load, we stretch and hold the lap-shear specimens at a certain strain for an extended period of time (Figure 3.2c).

The load and the extension of the crack are recorded throughout the test (up to 3 hours). The applied strains are lower than that to initiate fast debonding (ε_c~0.5). As expected, we observe the load relaxes over time due to the viscoelasticity of the adhesive matrix [27] and the skin [28]. Interestingly, no crack extension is observed under our testing conditions (G = 174.5 Jm^{-2} and 229.4 Jm^{-2}), though they approach the critical condition for fast debonding. The initial crack remains stationary indefinitely in our tests, in contrast to the delayed fracture phenomena observed on bulk hydrogels [19]. The tests confirm with us the range of applied strains where no static fatigue occurs, and in which we explore the effect of cyclic fatigue fracture as follows.

3.3.3. Cyclic fatigue tests

We next study the crack extension under prolonged cyclic loading. The modified lap-shear specimens are stretched cyclically with a triangular strain profile (frequency 1 Hz unless specifying). The choice of frequency is based on the limit of displacement rate of the Instron machine and an attempt to mimic the typical deformation frequency of biological tissues such as lung (0.2-0.3 Hz [18]) and heart (~1.0 Hz [29]). The strain is cycled between 0 and a maximum value ε below the critical strain for fast debonding (Figure 3.3a). The tests stop at 330,000 cycles or when the crack propagates through the interface. The load and the crack extension are recorded throughout the test. With known loads and strains, we can calculate the energy release rate as a function of the number of cycles.

Shakedown

We observe that the TA-skin specimens exhibit shakedown under cyclic load, similar to bulk hydrogels [20]. It is manifested as the gradual decrease of the maximum load and the area of the hysteresis loop as a function of the number of cycles (Figure 3.3b-d). The long-termed characteristics of the shakedown behavior depend on the magnitude of the applied strain. Under a relatively large strain (ε = 0.375), the initial crack grows progressively and runs through the entire interface (Figure 3.10). As a result, the ability of the adhesive joint to carry cyclic load is lost

within 5,000 cycles; in contrast, the same joint can sustain the static load of the same magnitude over time as shown above (Figure 3.2d).

Under intermediate strains (ε = 0.225, 0.25), the maximum load drops rapidly initially then reaches a steady-state over 10,000 cycles (Figure 3.3b), accompanying a gradual extension of crack. Under small strains (ε = 0.125, 0.175), the maximum load approaches a steady state, but no crack extension is observed. The load-strain curves reveal large areas of hysteresis loops in the first few cycles and then become elastically in the steady-state (Figure 3.3c&d). The observed shakedown generally accounts for both the crack advancing at the interface and the energy dissipating processes in the specimen including breaking of ionic cross-links within the TA matrix and the viscoelasticity of the skin [28]. But it is due to the energy dissipation under small strains (ε < 0.25) since the crack doesn't propagate throughout the test. When the energy dissipating events get depleted and the load is eventually carried with the elastic substructures in the specimen (i.e., the PAAM network), the hysteresis becomes negligible and the load-strain curve reaches a steady-state (Figure 3.3c). For instance, at the 10,000th and 20,000th cycle, the load-strain curves are almost the same, i.e., the TA-skin interface has shaken down. The finding is in accord with the recent studies on the fatigue of bulk hydrogels [20].

To further confirm the existence of the steady-state and to examine the frequency dependence of the shakedown behavior, we vary the loading frequency from 1 Hz to 0.5 Hz with fixed applied strain ε=0.125 (Figure 3.3c and 3.3d), in this case, the crack didn't propagate. In the first few cycles, the load-strain curves are different, indicative of the rate-dependent nature of the energy dissipating events (e.g., bond breaking and viscoelasticity). The difference becomes subtle when the load-strain curves reach the steady-state, indicating the response of the elastic substructures of the specimen. The maximum loads at either frequency approach 250 Nm^{-1} at the 20000th cycle. The results confirm that the shakedown behavior is attributed to the energy dissipating events under zero or small rates of crack extension and the lap-shear specimen can bear certain mechanical load indefinitely over cycles.

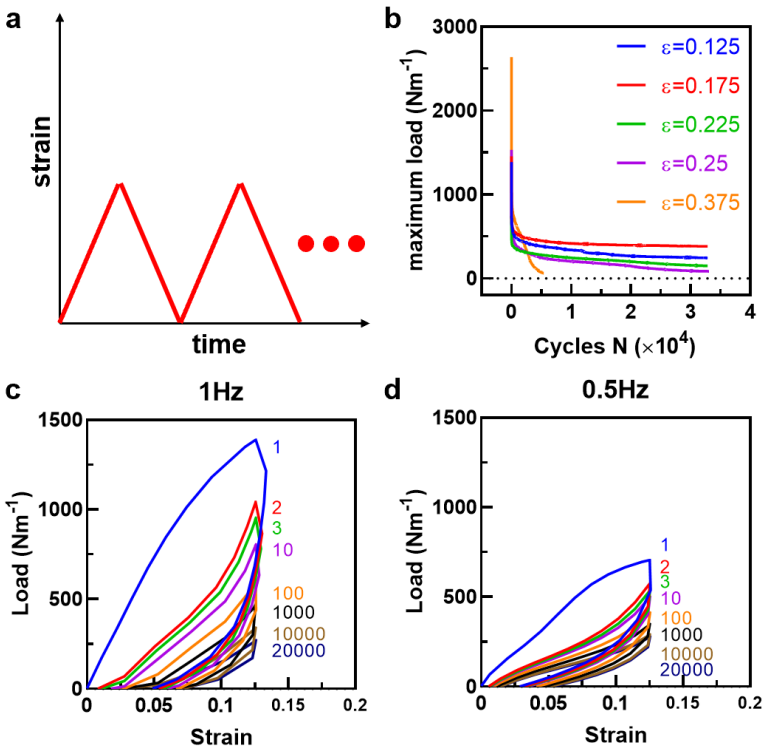

Figure 3.3 Shakedown under cyclic load. (a) Schematic profile of cyclic load. (b) Maximum load decreases with cycles and approaches a steady state. The applied strains are varied. Shakedown phenomena under different frequencies with fixed applied strain ε=0.125: 1 Hz (c) and 0.5 Hz (d). The tests are performed with displacement control. The displacement is cycled between 0 and the maximum prescribed value. The strain is defined as $\varepsilon = d/L$. The cycle numbers are as labelled.

Interfacial fatigue fracture

We next characterize the crack extension under cyclic load. The crack extension Δc is plotted as a function of the number of cycles N (Figure 3.4a). In our tests, the initial crack always extends along with the interface between the TA and the skin. No crack kinking is observed. Figure 3.4a shows three crack extension behaviors: At large strain (ε = 0.375), the crack extends rapidly; at intermediate strains (ε = 0.225, 0.25), the crack extends slowly as the cycle number increases; at small strains, the crack either remains stationary (ε = 0.125) or stops after small extension in the first few cycles (ε = 0.175).

To quantify the effect of mechanical load on crack extension, we report the amplitude of load in terms of the energy release rate G. When calculating the G using the equation shown above, we need to map the applied strains (i.e., the displacement divided by the real overlap length as crack growing) and the load-strain curves at each cycle. Because the crack length may vary with cycles and the load-strain curves shake down. When plotting Figure 3.4c, we calculate the crack growth rate dc/dN by normalizing the crack extension with the cycle number increment between two adjacent data points in Figure 3.4a and average the energy release rate G at the corresponding cycles in Figure 3.4b (see details in Supporting Information). We choose this method instead of a linear fitting method because the crack extension curves are highly nonlinear (Figure 3.4a) and the cycle intervals (10,000 cycles) are sufficiently large. Under most of the testing conditions ($\varepsilon < 0.375$), the G decreases and reaches a steady value after ~10,000 cycles. Notably, the G remains stable during the process of slow crack propagation ($\varepsilon = 0.225$), as the load decreases and the real strain increases coordinately.

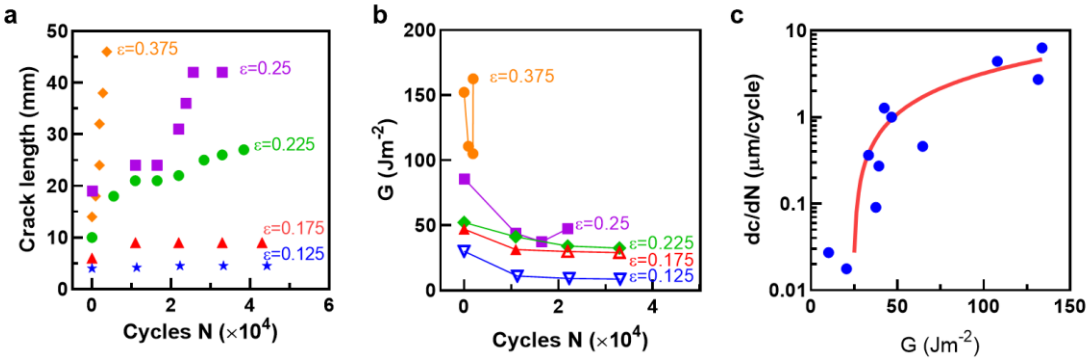

Figure 3.4 Fatigue fracture characterization. (a) Crack lengths as a function of the number of cycles N and the applied strains ε. (b) Energy release rate as a function of the number of cycles N. (c) Extension of crack per cycle is plotted as a function of energy release rate G. A threshold is estimated between two points of the lowest crack growth rate. A red line is a linear regression of the experimental data.

Interfacial fatigue threshold

With the G-N plot, we plot the crack extension rate dc/dN as a function of the energy release rate G (Figure 3.4c). We calculate dc/dN from the Δc-N curves and map the corresponding G. From the dc/dN-G curve, we estimate the threshold for interfacial fatigue fracture Γ_o with a linear regression method following a method

reported previously [20]. From our measurements, we find the interfacial fatigue threshold for the TA-skin interface is 24.4 Jm^{-2}. This value is much lower than the adhesion energy (~580 Jm^{-2}) for fast debonding measured under monotonic load (Figure 3.2b). Indeed, the results are consistent with the previous reports on the fatigue of bulk hydrogels, where the fatigue threshold is typically much lower than the fracture energy. Similar to the fatigue of bulk hydrogels, this finding can be understood that the fatigue threshold depends primarily on the covalently cross-linked network bridging between the adhesive and the skin. The toughening mechanisms like the breaking of Ca-alginate bonds contribute little to the fatigue threshold, despite its potent improvement on the adhesion energy. It is worthwhile to note that the interfacial fatigue threshold is obtained under a fixed cycling rate (frequency 1 Hz); the potential frequency dependence requires further investigation to explore.

The interfacial fatigue threshold has practical significance. If the mechanical load is below the threshold, the TA-skin interface is immune to the cyclic loading and the adhesive can theoretically sustain an infinite number of cycles without debonding. Although the threshold of the TA is lower than its adhesion energy, the value of the fatigue threshold remains larger than the adhesion energy (1-10 Jm^{-2}) of many existing tissue adhesives, including nanoparticles [30], clinically used surgical glues and bandages [12]; it can be attributed to the fact that the long-chain chitosan enables the interfacial bonding (i.e., amide bonds) of high density and large bond energy between the adhesive and the skin. The result implies that TA can sustain infinite cycles of the mechanical loading of the magnitude that can fail the other tissue adhesives at one loading. This study reveals the need to develop fatigue-resistant tissue adhesive with high interfacial fatigue threshold. To this end, it is appealing to explore composite tissue adhesives with fiber reinforcement, as recent progresses show that the composite strategy increases the fatigue threshold of bulk hydrogels to 1000 Jm^{-2} [31,32].

Comparison with the fatigue of bulk hydrogels

To reveal the underlying mechanism of the interfacial fatigue fracture, we next compare the fatigue of the TA-skin interface with the fatigue of TA-hydrogel interface and bulk hydrogels. We replace the skin with the alginate-polyacrylamide hydrogel as adherend for the cyclic fatigue tests. As the hydrogel is identical to the matrix of TA, the TA-hydrogel specimen mimics a bulk alginate-polyacrylamide tough hydrogel to some extent. Figure 3.5a shows that under the same cyclic strain, the crack growth at the TA-hydrogel interface is slower than that at the TA-skin interface. The effect can be attributed to the toughening mechanism of the hydrogel adherend, which helps dissipate more energy than the skin and thus slow down the crack growth. As the hydrogel adherend can better facilitate the diffusion of the bridging polymer and the formation of covalent bonds at the interface, we hypothesize the fatigue threshold of the TA-hydrogel interface would be larger than that of the TA-skin interface. Indeed, our result shows Γ_o at 31.3 J m^{-2} measured with the same method above. The threshold of the TA-hydrogel interface is slightly larger than that of the TA-skin interface.

Figure 3.5b compares the TA-skin interface with the TA-hydrogel interface and the bulk hydrogel in terms of the fatigue fracture behavior. The data associated with the bulk hydrogels is extracted from a recent report where an alginate-polyacrylamide tough hydrogel of compositions similar to the matrix of TA was tested with cyclic load under pure-shear configuration [20]. Figure 3.5b shows that the interfacial crack growth is faster than that occurs in the bulk hydrogel and that the fatigue threshold of bulk hydrogel (~50 J m^{-2}) is larger than those measured at the interface. We conjecture that it is due to the difference of primary networks at the crack tip: the chitosan-based bridging network at the interface is not as strong as the polyacrylamide network in the bulk hydrogel. The fatigue thresholds reflect the chemical networks participating in the fracture process. It is important to note the different loading modes used here and in the previous study on bulk hydrogels. The loading mode is known to affect the fatigue crack extension in metals [33],

polymers [34] and ceramics [35]. It deserves further investigation but is out of the scope of this study.

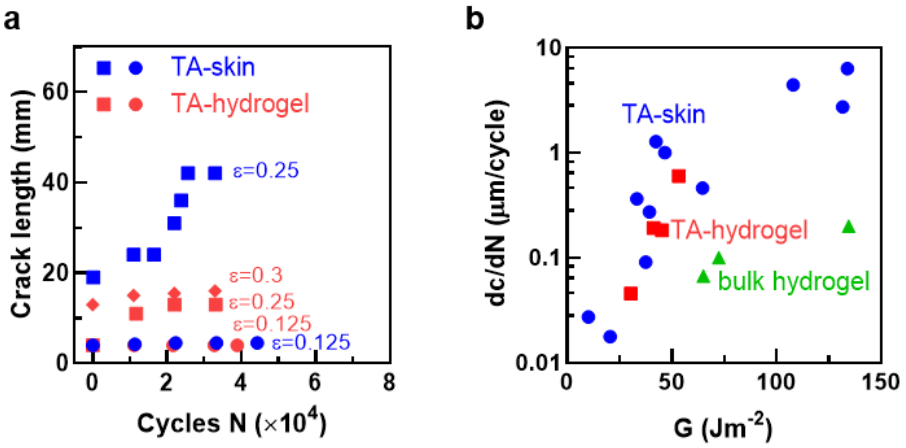

Figure 3.5 Comparison with interfacial and bulk fatigue fracture. (a) Crack lengths at the TA-skin and TA-hydrogel interfaces as a function of the number of cycles N. (b) Crack growth rate as a function of energy release rate G.

The Lake-Thomas model has been adopted to predict the fatigue threshold of hydrogels [19,21,22,36,37]. According to this model, we depict that a bridging network consisting of covalently cross-linked alginate and chitosan contributes to the fatigue threshold and the crack only disassociates the polymer chains ahead of the crack lying across the crack plane when the applied load is above the fatigue threshold. The average number *n* of monomers per chains of the bridging network is difficult to measure, unlike the bulk hydrogel where n is often determined from the shear modulus. Thus, we approximate n with the segment number (~1000) of the bridging polymers. The intrinsic fatigue threshold is thus calculated via [19]

$$\Gamma_0 = \phi^{\frac{2}{3}} bUl\sqrt{n}$$

where ϕ is the volume fraction of the chitosan and alginate, b is the average number of inter-monomer C-O bonds per unit volume of the chitosan and alginate in a dry state, U is the C-O bond energy, and l is the average length of each segment unit. The analysis gives the threshold of interfacial fatigue 5 Jm^{-2} (see details in Supporting Information), much lower than the experimentally measured value of 24.4 Jm^{-2}. A similar discrepancy is reported in a recent report on the

fatigue of tough hydrogels, showing that the theoretical and experimentally measured fatigue thresholds are 9.1 Jm^{-2} and 35 Jm^{-2}, respectively [36]. The result implies that entanglements and other polymer interactions might contribute to the fatigue threshold, which is not considered in the Lake-Thomas theory.

3.4. Conclusion

To sum up, we presented a systematic study on the interfacial fracture of tough adhesives on skin. We tested three kinds of loading: monotonic, static and cyclic loads and observed fast debonding and interfacial fatigue fracture. Under cyclic load, the load-strain curve exhibited substantial shakedown over cycles. We characterized the crack growth rate as a function of the energy release rate. The threshold for the interfacial fatigue fracture was measured at 24 Jm^{-2}, below which no crack extension at the TA-skin interface was observed. The fatigue threshold was much lower than the adhesion energy of the TA for fast debonding but remained higher than the adhesion energy of commercially available surgical adhesives and bandages (1-10 Jm^{-2}). By comparing with the fatigue of bulk hydrogel, we also showed that the crack extension rate at the interface was higher than that in the bulk hydrogel and that the interfacial fatigue threshold was lower than the fatigue threshold of the bulk hydrogel. Our study answered fundamental questions regarding the interfacial fatigue of tissue adhesive hydrogels. It is hoped that this study would stimulate more study on the interfacial fracture of tissue adhesives and promote the development of tissue adhesives of high fatigue threshold.

3.5. Acknowledgments

Funding: This work was supported by Natural Sciences and Engineering Research Council of Canada (grants RGPIN-2018-04146 and EGP 538388-19), Canada Foundation for Innovation (grant 37719) and New Frontiers in Research Fund (NFRF) Exploration Grant (NFRFE-2018-00751).

Author contributions: X.N. and J.L. conceived and designed the study. X.N. conducted the experiments. C.C. and J.L. developed the theoretical framework to calculate the energy release rate. X.N., C.C., and J.L. analyzed the results and wrote the manuscript.

Competing interests: The authors declare that they have no competing interests regarding this work.

Data and materials availability: All data needed to evaluate the conclusions in the paper are present in the paper and/or the Supplementary Materials. Additional data related to this paper may be requested from the authors.

3.6. References

[1] J.M. Karp, A slick and stretchable surgical adhesive, N. Engl. J. Med. 377 (2017) 2092–2094.

[2] R. Pinnaratip, M.S.A. Bhuiyan, K. Meyers, R.M. Rajachar, B.P. Lee, Multifunctional biomedical adhesives, Adv. Healthc. Mater. (2019) 1801568.

[3] J. Li, A.D. Celiz, J. Yang, Q. Yang, I. Wamala, W. Whyte, B.R. Seo, N. V Vasilyev, J.J. Vlassak, Z. Suo, D.J. Mooney, Tough adhesives for diverse wet surfaces, Science 357 (2017) 378–381.

[4] M.W. Grinstaff, Designing hydrogel adhesives for corneal wound repair, Biomaterials. 28 (2007) 5205–5214.

[5] N. Lang, M.J. Pereira, Y. Lee, I. Friehs, N. V Vasilyev, E.N. Feins, K. Ablasser, E.D. O'Cearbhaill, C. Xu, A. Fabozzo, A blood-resistant surgical glue for minimally invasive repair of vessels and heart defects, Sci. Transl. Med. 6 (2014) 218ra6.

[6] N. Annabi, Y.N. Zhang, A. Assmann, E.S. Sani, G. Cheng, A.D. Lassaletta, A. Vegh, B. Dehghani, G.U. Ruiz-Esparza, X. Wang, S. Gangadharan, A.S. Weiss, A. Khademhosseini, Engineering a highly elastic human protein-based sealant for surgical applications, Sci. Transl. Med. 9 (2017) eaai7466.

[7] M. Mehdizadeh, J. Yang, Design strategies and applications of tissue bioadhesives, Macromol. Biosci. 13 (2013) 271–288.

[8] Y. Liu, H. Meng, Z. Qian, N. Fan, W. Choi, F. Zhao, B.P. Lee, A moldable nanocomposite hydrogel composed of a mussel‐inspired polymer and a nanosilicate as a fit‐to‐shape tissue sealant, Angew. Chemie Int. Ed. 56 (2017) 4224–4228.

[9] M.R. Prausnitz, R. Langer, Transdermal drug delivery, Nat. Biotechnol. 26 (2008) 1261-1268.

[10] J. Li, D.J. Mooney, Designing hydrogels for controlled drug delivery, Nat. Rev. Mater. 1 (2016) 16071.

[11] E.T. Roche, M.A. Horvath, I. Wamala, A. Alazmani, S.-E. Song, W. Whyte, Z. Machaidze, C.J. Payne, J.C. Weaver, G. Fishbein, Soft robotic sleeve supports heart function, Sci. Transl. Med. 9 (2017) eaaf3925.

[12] S.O. Blacklow, J. Li, B.R. Freedman, M. Zeidi, C. Chen, D.J. Mooney, Bioinspired mechanically active adhesive dressings to accelerate wound closure, Sci. Adv. 5 (2019) eaaw3963.

[13] L. Han, X. Lu, K. Liu, K. Wang, L. Fang, L.-T. Weng, H. Zhang, Y. Tang, F. Ren, C. Zhao, Mussel-inspired adhesive and tough hydrogel based on nanoclay confined dopamine polymerization, ACS Nano 11 (2017) 2561–2574.

[14] Y. Gao, K. Wu, Z. Suo, Photodetachable adhesion, Adv. Mater. 31 (2019) 1806948.

[15] H. Yang, C. Li, J. Tang, Z. Suo, Strong and degradable adhesion of hydrogels, ACS Appl. Bio Mater. 2 (2019) 1781-1786.

[16] L. V Gulotta, D. Kovacevic, L. Ying, J.R. Ehteshami, S. Montgomery, S.A. Rodeo, Augmentation of tendon-to-bone healing with a magnesium-based bone adhesive, Am. J. Sports Med. 36 (2008) 1290–1297.

[17] H.J. Levine, Rest heart rate and life expectancy, J. Am. Coll. Cardiol. 30 (1997) 1104–1106.

[18] K.E. Barret, S. Boitano, S.M. Barman, Ganong's review of medical physiology, McGraw-Hill Education 24 (2012).

[19] J.D. Tang, J.Y. Li, J.J. Vlassak, Z.G. Suo, Fatigue fracture of hydrogels, Extrem. Mech. Lett. 10 (2017) 24–31.

[20] R.B. Bai, Q.S. Yang, J.D. Tang, X.P. Morelle, J. Vlassak, Z.G. Suo, Fatigue fracture of tough hydrogels, Extrem. Mech. Lett. 15 (2017) 91–96.

[21] W. Zhang, X. Liu, J. Wang, J. Tang, J. Hu, T. Lu, Z. Suo, Fatigue of double-network hydrogels, Eng. Fract. Mech. 187 (2018) 74–93.

[22] R.B. Bai, J.W. Yang, X.P. Morelle, C.H. Yang, Z.G. Suo, Fatigue fracture of self-recovery hydrogels, ACS Macro Lett. 7 (2018) 312–317.

[23] A. Pirondi, F. Moroni, An investigation of fatigue failure prediction of adhesively bonded metal/metal joints, Int. J. Adhes. Adhes. 29 (2009) 796–805.

[24] F. Campos, L.F. Valandro, S.A. Feitosa, C.J. Kleverlaan, A.J. Feilzer, N. de Jager, M.A. Bottino, Adhesive cementation promotes higher fatigue resistance to zirconia crowns, Oper. Dent. 42 (2016) 215–224.

[25] W. Zielecki, A. Kubit, T. Trzepieciński, U. Narkiewicz, Z. Czech, Impact of multiwall carbon nanotubes on the fatigue strength of adhesive joints, Int. J. Adhes. Adhes. 73 (2017) 16–21.

[26] X. Zhao, Multi-scale multi-mechanism design of tough hydrogels: building dissipation into stretchy networks, Soft Matter 10 (2014) 672–687.

[27] R. Bai, B. Chen, J. Yang, Z. Suo, Tearing a hydrogel of complex rheology, J. Mech. Phys. Solids 125 (2019) 749–761.

[28] X. Zhang, R.R. Kinnick, M.R. Pittelkow, J.F. Greenleaf, Skin viscoelasticity with surface wave method, IEEE Internat. Ultrasonics Symp. (2008) 651–653.

[29] J.E. Hall, Guyton and Hall textbook of medical physiology, Elsevier Canada 12 (2011).

[30] S. Rose, A. Prevoteau, P. Elzière, D. Hourdet, A. Marcellan, L. Leibler, Nanoparticle solutions as adhesives for gels and biological tissues, Nature. 505 (2014) 382.

[31] S.T. Lin, X.Y. Liu, J. Liu, H. Yuk, H.C. Loh, G.A. Parada, C. Settens, J. Song, A. Masic, G.H. McKinley, X.H. Zhao, Anti-fatigue-fracture hydrogels, Sci. Adv. 5 (2019) eaau8528.

[32] C. Xiang, Z. Wang, C. Yang, X. Yao, Y. Wang, Z. Suo, Stretchable and fatigue-resistant materials, Mater. Today. (2019) DOI: 10.1016/j.mattod.2019.08.009.

[33] E.K. Tschegg, Mode III and mode I fatigue crack propagation behaviour under torsional loading, J. Mater. Sci. 18 (1983) 1604–1614.

[34] D. Grégoire, H. Maigre, J. Rethore, A. Combescure, Dynamic crack propagation under mixed-mode loading–comparison between experiments and X-FEM simulations, Int. J. Solids Struct. 44 (2007) 6517–6534.

[35] A.G. Evans, E.R. Fuller, Crack propagation in ceramic materials under cyclic loading conditions, Metall. Trans. 5 (1974) 27.

[36] W. Zhang, J. Hu, J. Tang, Z. Wang, J. Wang, T. Lu, Z. Suo, Fracture toughness and fatigue threshold of tough hydrogels, ACS Macro Lett. 8 (2018) 17–23.

[37] E.R. Zhang, R.B. Bai, X.P. Morelle, Z.G. Suo, Fatigue fracture of nearly elastic hydrogels, Soft Matter 14 (2018) 3563–3571.

3.7. Supporting Information

3.7.1. Sample Preparation

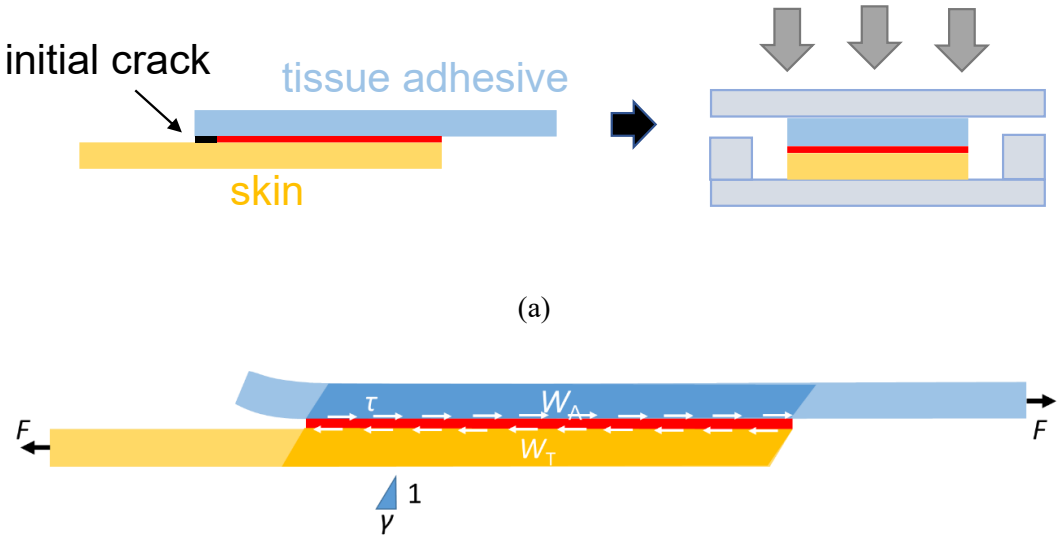

Figure 3.6 Schematics of specimen preparation. (a) An edge crack is introduced at the interface of the tissue adhesive and the skin (Left). Gentle compression is applied to form the adhesion (Right). (b) Specimen undergoes shear deformation under lap shear.

3.7.2. Experimental Setup

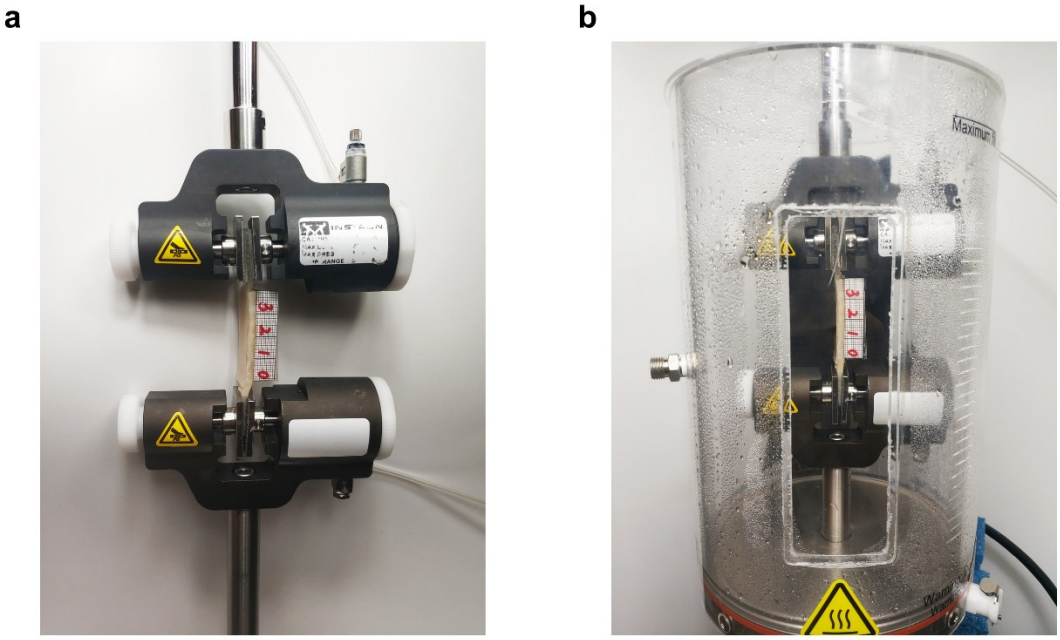

Figure 3.7 Experimental setup for humidity control. (a) A digital image of a clamped specimen with an attached ruler line. (b) A closed chamber maintains high humidity and prevents the specimen from dehydration.

3.7.3. Tensile Curves of Tough Hydrogel and Skin

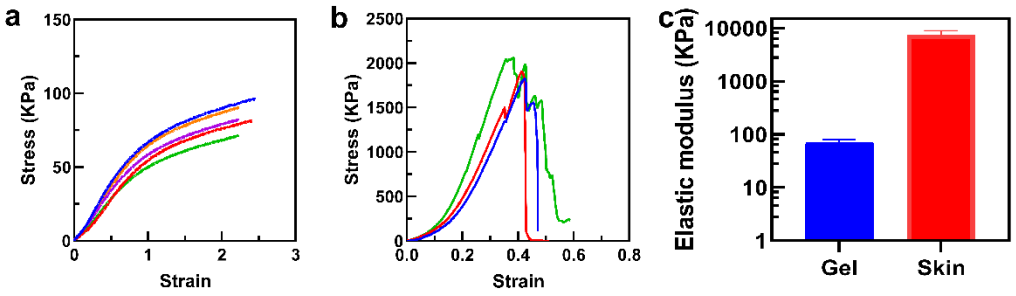

Figure 3.8 Tensile stress-strain curves of the adhesive and the skin. (a) Stress-strain curves of the adhesive matrix made of alginate-polyacrylamide tough hydrogel. (b) Stress-strain curves of the porcine skin. Multiple specimens are tested and color-coded. (c) Elastic moduli of the adhesive matrix and the skin. Sample size N=3-5.

3.7.4. Loading Curves of Lap Shear and Simple Shear Tests

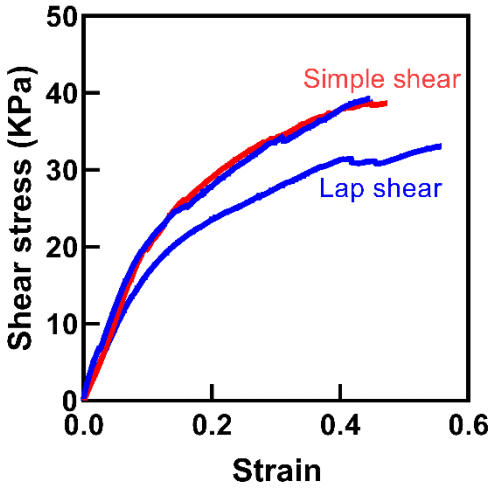

Figure 3.9 Stress-strain curves under lap shear and simple shear loading.

3.7.5. Digital Images of Cyclic Fatigue Failure

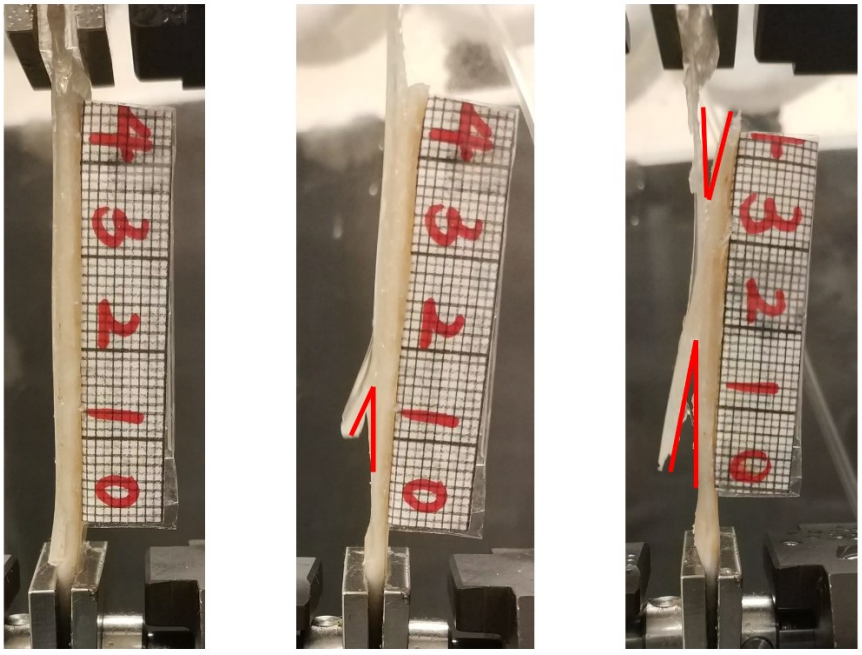

Figure 3.10 Digital images of the specimen under cyclic loading. The crack surface is highlighted in red and the cycle number (N) is indicated below.

3.7.6. Mass Change of Specimen

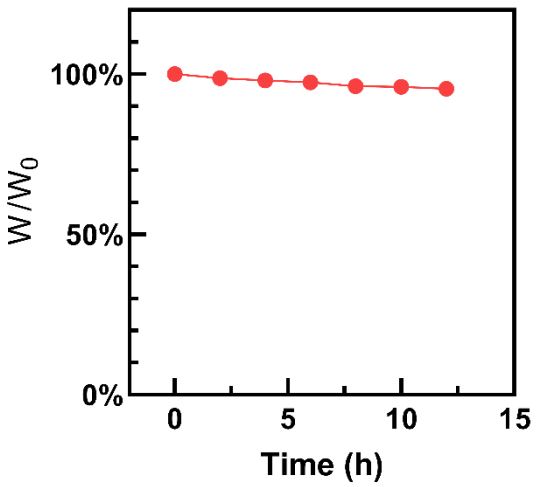

Figure 3.11 Mass change of specimen in a closed chamber over time. W_0 denotes initial weight. Water loss of specimen is within 5% in 12 hours.

3.7.7. Derivation of Energy Release Rate G

A stripe of tissue adhesive and a stripe of adherend of the same width *w* are adhered to form a joint length *L*. An initial crack with length c was introduced before the test. The thicknesses of the adhesive and the tissue are t_A and t_T, respectively. Both the adhesive and the adherend are supported with rigid PET films to prevent the elongation of materials in the pulling direction.

Upon stretching, the interface of the joint bears the shear stress,

$$\tau = F/(wL), \qquad \text{(S1)}$$

presumably that the distribution of shear stress over the joined region is uniform. Figure 3.6b shows that the joint parts thus are in a simple shear state with shear strain γ_A and γ_T, indicating the tangents of shear angles of the adhesive and the tissue, respectively. The integration of shear stress over the shear strain defines the strain energy density stored at the joint parts,

$$W_i(\gamma_i) = \int \tau d\gamma_i , \quad \text{(S2)}$$

where the subscript *i* represents the adhesive with *A*, and the tissue with *T*. Meanwhile, the unjointed part, subject to the constraint from rigid backing films, their deformation is negligible. The deformation of the transition from joint parts to unjoint parts is complicated but remains constant over an infinitesimal growth of the crack. Therefore, its contribution to the energy release rate is nulled. Considering a constant force loaded, the free energy includes the potential energy of the load, *-Fd*, where *d* is the displacement between loading ends was caused by the shear of the shear-lap region, i.e., $t_A\gamma_A + t_T\gamma_T$. The total free energy of the system is:

$$\Pi = W_A t_A L w + W_T t_T L w - F\left(t_A\gamma_A + t_T\gamma_T\right) \quad \text{(S3)}$$

We allow the crack length *c* extends, which reduces the joint length *L* with the same amount. We determine the energy release rate by $-\partial\Pi/\left(w\partial c\right)$, or equivalently, by

$$G = \frac{\partial\Pi}{w\partial L} . \quad \text{(S4)}$$

Combining with Eq. S1-S3 into Eq. S4 yields:

$$\begin{aligned} G = & W_A t_A + \tau\frac{\partial\gamma_A}{\partial\tau}\left(-\frac{\tau}{L}\right)t_A L + W_T t_T + \tau\frac{\partial\gamma_T}{\partial\tau}\left(-\frac{\tau}{L}\right)t_T L \\ & -\frac{F}{w}\left(t_A\frac{\partial\gamma_A}{\partial\tau} + t_T\frac{\partial\gamma_T}{\partial\tau}\right)\left(-\frac{\tau}{L}\right) \\ = & W_A t_A + W_T t_T \end{aligned}$$

3.7.8. Mapping Δc-N and G-N Curve to dc/dN-G Curve

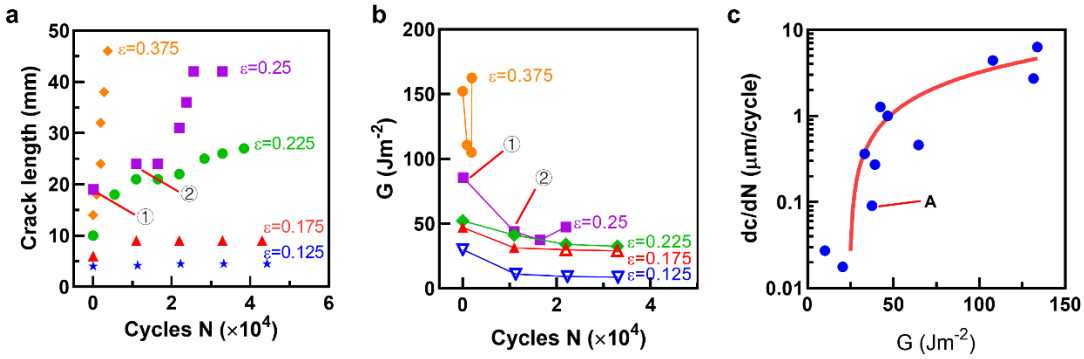

Figure 3.12 Fatigue fracture characterization. (a) Crack lengths as a function of the number of cycles N and the applied strains ε. (b) Energy release rate as a function of the number of cycles N. (c) Extension of crack per cycle is plotted as a function of energy release rate G. A threshold is estimated between two points of the lowest crack growth rate. A red line is a linear regression of the experimental data.

We map adjacent two points in Figure 3.12a&b to the corresponding point in Figure 3.12c. For example, the crack length difference divided by the cycle number increment between point ① and ② in Figure 3.12a is the ordinate of point A in Figure 3.12c. The mean G of point ① and ② in Figure 3.12b is the abscissa of point A in Figure 3.12c.

3.7.9. Estimating the fatigue threshold using Lake-Thomas model

According to the Lake-Thomas model, the theoretical fatigue threshold takes the form

$$\Gamma_0 = \Phi^{2/3} b U l \sqrt{n}$$

Where Φ is the volume fraction of the polymers in hydrogel, b is the number of inter-segment bonds per unit volume of the dry polymer, U is the bond energy, l is the length of each monomer unit and n is the number of monomer units in a polymer chain. In the case of the tough adhesive hydrogels, we have

$$\Phi_{\text{alginate}} = \frac{(1\text{-}W_{\text{water}}) \times \frac{m_{\text{alginate}}}{m_{\text{PAAm}} + m_{\text{alginate}}}}{\rho_{\text{alginate}}} \times \rho_{\text{gel}}$$

$$\Phi_{\text{chitosan}} = \frac{m_{\text{chitosan}}/\rho_{\text{chitosan}}}{m_{\text{mixture}}/\rho_{\text{mixture}}}$$

where m is the mass, ρ is the density, the subscriptions denote alginate and chitosan respectively. The density of both alginate and chitosan is 1.6 g/cm^3. The density of the mixture solution is 1 g/cm^3. The volume fraction of alginate Φ_{alginate} is 1.22 vol%, the volume fraction of chitosan chains in the mixture solution Φ_{chitosan} is 1.25 vol%. The ratio of alginate versus chitosan is 0.0932 : 0.0955. The average number of inter-segment bonds per unit volume of the dry polymer is estimated by the average number of monomers per volume of the dry polymer, $b = \frac{A\rho_{\text{alginate}}}{M_{\text{G residue}}} \times 0.0932 + \frac{A\rho_{\text{chitosan}}}{M_{\text{glucosamine}}} \times 0.0955 = 5.4 \times 10^{27} m^{-3}$, where A is the Avogadro number (6.022 × 10^{23}) and M is the unit molecular weight of alginate (176 g/mole) and chitosan (179.172 g/mole). The energy of a C-O bond $U_{C\text{-}O}$ is 6.1 × 10^{-19} J. The length of the monomer is estimated by $l = (b)^{-1/3} = 0.57\ \text{nm}$. The number of monomer units in a bridging polymer chain n is around 1000. Accordingly, the fatigue threshold of tissue adhesive hydrogel is predicted to be 5.04 Jm^{-2}.

Chapter 4. Article 2: Scaling Behavior of Fracture Properties of Tough Adhesive Hydrogels

Xiang Ni, †‡ Zhen Yang, †‡ Jianyu Li†§*

† Department of Mechanical Engineering, McGill University, Montreal, QC H3A 0C3, Canada

§ Department of Biomedical Engineering, McGill University, Montreal, QC H3A 0C3, Canada

Abstract

Tough adhesive hydrogels find broad applications in engineering and medicine. Such hydrogels feature high resistance against both cohesion and adhesion failure. The superior fracture properties may, however, deteriorate when the hydrogels swell upon exposure of water. The underlying correlation between the polymer fraction and fracture properties of tough adhesive hydrogels remains largely unexplored. Here we study how the cohesion and adhesion energies of a tough adhesive hydrogel evolve with the swelling process. The results show a similar scaling law (ϕ^{υ}) of the two quantities as a function of the polymer fraction (ϕ). Our scaling analysis and computational study reveal that it stems from the scaling of shear modulus. The study will promote the investigation of scaling of hydrogel fracture and provide development guidelines for next-generation tough adhesive hydrogels.

4.1. Introduction

Tough adhesive hydrogels are highly resistant to crack growth within the matrix, and capable of adhering strongly to diverse substrates such as biological tissues and elastomers [1,2]. The tough adhesive hydrogels are in contrast to conventional hydrogels, which are vulnerable to cohesion failure (*i.e.*, fracture in the bulk) and adhesion failure (*i.e.*, debonding at the interface). Thanks to the exceptional properties, tough adhesive hydrogels open a plethora of applications such as

tissue adhesives [3,4], wound dressings [5], soft robotics [6,7], and implantable devices [8,9]. In many applications, the hydrogels are exposed to water and readily swell. The resulting change of the polymer fraction (*i.e.*, the water content) may significantly alter the fracture properties of the hydrogels [10]. The underlying correlation is thus fundamental and practically important to explore.

The coupling between the swelling and fracture of tough adhesive hydrogels poses challenges to theoretical analysis [11,12], and computational modeling [13,14]. It is in part because both the cohesion and adhesion failure of tough adhesive hydrogels involve stress/strain fields of highly nonlinear nature and complex physicochemical interactions. To this end, the scaling theory by de Gennes [15] and many others is appealing. Because it can capture key structure-property relations, such as the dependence of elastic modulus and polymer content, to reveal the fundamentals and enable material design. However, few reports have been seen on the scaling of fracture properties (*e.g.*, cohesion and adhesion energies). One exception is a recent work, reporting the elastic modulus and the intrinsic cohesion energy (*i.e.*, intrinsic toughness with no background hysteresis involved) of polyacrylamide hydrogels scale in the same way as a function of the polymer fraction [16]. In the case of tough adhesive hydrogels, the fracture properties (either cohesion or adhesion) are dominated by background hysteresis, whereas the intrinsic toughness plays a minor role (Figure 4.4) [17]. Little is known about the scaling of the polymer fraction and the cohesion and adhesion energies, which is the focus of the current study. We will swell the tough adhesive hydrogels for varying polymer fractions and then characterize their cohesion and adhesion energies, respectively. The results will be further analyzed with a scaling theory developed by Brown [18] and finite element (FE) simulation. This work would lead to insights and experimental methods to control and predict the mechanics of tough adhesive hydrogels.

4.2. Results and Discussion

In this study, we choose an alginate-polyacrylamide hydrogel as the model hydrogel and porcine skin as the model substrate [19]. The hydrogel is extremely tough and can form tough adhesion on various substrates, including hydrogels and tissues, using recently developed strategies [1,2,20]. We synthesized and swelled the alginate-polyacrylamide hydrogels in PBS for different durations (0-6 hours). The PBS is chosen to mimic the physiological environment in biomedical applications of tissue adhesive hydrogels. Note that, in addition to the swelling, the ionic crosslinks of the hydrogel can dissociate due to the ion exchange with the solution. The resulting hydrogels with varying polymer fractions were then placed in a sealed bag for a homogeneous water distribution inside (Figure 4.1a). We then activated the hydrogel surface with chitosan and EDC/NHS, and compressed the hydrogel to porcine skin to form tough adhesion[1]. We measured the weight of the wet gel and that of solid content after lyophilization, and then calculated the polymer fraction ϕ (See Experimental Methods). With longer swelling, the hydrogels absorb more water and further lower the polymer fraction (Figure 4.5), which can be varied between 5% and 10%. In addition to the change of the polymer fraction, the nominal crosslink density of the Alginate-Ca^{2+} network was progressively dissociated upon swelling, due to the ion exchange between the hydrogel and PBS.

Next, we characterize the cohesion energy and adhesion energy of the swollen hydrogels using tear and 180-degree peeling methods, respectively. The tear testing has been widely used to measure cohesion energy (*i.e.*, toughness) of materials such as hydrogels [21] and elastomers [22], and is chosen in this study to ensure crack propagation through the bulk matrix. While the arms of the specimen are pulled unidirectionally at a constant speed, the pulling force increases to a plateau (Figure 4.1b-d). The averaged plateau force F is used to calculate the cohesion energy via $\Gamma_C = 2F/t$. As expected, the cohesion energy decreases as the hydrogel matrix swells. We also characterize the adhesion energy between the tough adhesive hydrogel and the porcine skin with 180-degree

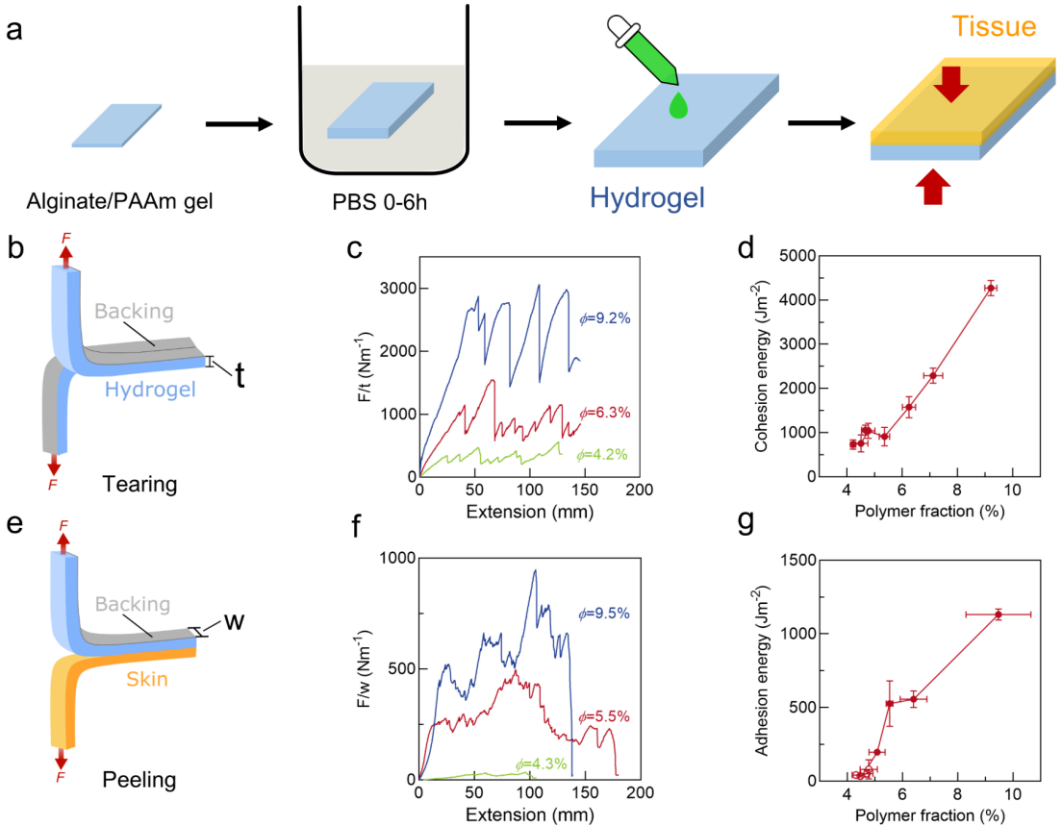

Figure 4.1 Fracture measurements of tissue adhesive hydrogels with varying polymer fractions. (a) As prepared alginate/PAAm hydrogels were soaked in PBS solutions for varying durations, then activated with chitosan and coupling agents to form adhesion with tissues under compression. (b-d) Cohesion energy measurement with tearing test. (b) A specimen of thickness t is pulled vertically with a constant speed. (c) Tearing force per thickness of hydrogels as a function of extension and polymer fraction. The region between 40 mm and 120 mm is considered as plateau and averaged to calculate cohesion energy. (d) Cohesion energy as a function of polymer fraction. (e-g) Adhesion energy measurement with 180-degree peeling test. The specimen width is w. (f) Peeling force per width as a function of extension and polymer fraction. The region between 40 mm and 120 mm is considered as plateau and averaged to calculate adhesion energy. (g) Adhesion energy as a function of polymer fraction, empty circles indicate weak bonding. Sample size N=3.

peeling tests (Figure 4.1e-g). From the peeling tests, the plateau peeling force is used to calculate the adhesion energy via $\Gamma_A = 2F/w$. Similar to the cohesion energy, the adhesion energy exhibits a positive correlation with the polymer fraction. Interestingly, when the polymer fraction is below 5%, no tough adhesion is formed. Because the adhesion is so weak that the interface debonds well before the two arms of the specimen are stretched to 180 degrees. The phenomenon can

be understood that the large mesh size of the swollen hydrogel exceeds the limit for the formation of entanglements between the chitosan chains and the hydrogel network at the interface, which has been shown critical for the tough adhesion of the hydrogel used in this work [1]. As a result, poor adhesion was observed in the extremely swollen hydrogel. To overcome this limit, there exist a variety of strategies to form direct chemical bonding between the substrate and the hydrogel matrix [2,23,24]. As such, the interfacial bonding is achieved without forming entanglements at the interface. Together, the results show that modulating the polymer fraction can tune cohesion and adhesion energies of tough adhesive hydrogels over a wide range, and that there is a positive correlation between the polymer fraction and the fracture properties.

We then study the quantitative scaling of the cohesion and adhesion energies as a function of the polymer fraction. Figure 4.2 plots the preceding results in a log-log scale, showing an exponent of 2.2 and an identical scaling law ($\phi^{2.2}$) for the cohesion and adhesion energies. First, we hypothesize the scaling relation is attributable to the dependence of elastic modulus on the polymer fraction. To test the hypothesis, we perform a scaling analysis based on the Brown's model for the fracture of double network hydrogels [18]. This model can be applied to the tough hydrogel in this study. Because our measurements confirmed that the elastic modulus E_1 at loading stage before yielding is much larger than that at unloading stage E_2 (Figure 4.6), meeting the key assumption of the Brown's model. It is worth noting that the 1st network (alginate) and the 2nd (polyacrylamide) both contribute to the initial regime of the stress-strain curve (slope E_1), but the former dominates since the 1st network (alginate) is much stiffer than the 2nd network (polyacrylamide). When the strain reaches a critical value ε_1, the 1st network undergoes progressive damage, as manifested by a yielding regime at a critical stress $\sigma_1 = E_1\varepsilon_1$ (region 2). When the sample is further loaded to the maximum strain ε_2, the 1st network damages completely, and the 2nd network bridges the crack and bears all the load. As such, the stress-strain curve undergoes an abrupt decrease to a stress level $\sigma_2 = E_2\varepsilon_2$ (region 3). After that, the 2nd network

dominates the unloading response with a slope E_2 (region 4). This model allows us to relate the cohesion energy (i.e., fracture energy) to the elastic modulus without invoking complex fields as follows.

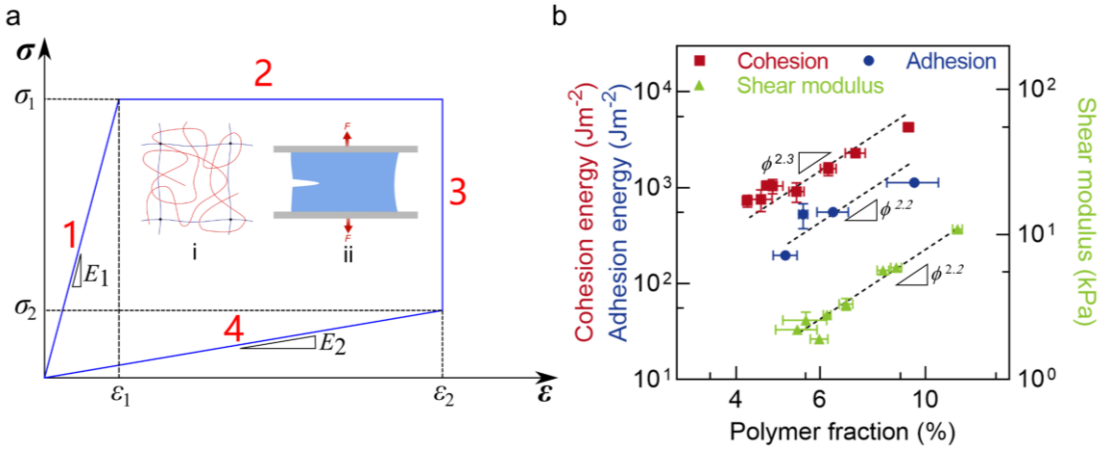

Figure 4.2 Scaling relations between mechanical properties and polymer fraction. (a) Tensile stress-strain curve of a loading-unloading cycle in Brown's model divided into 4 parts. Inserted figures: i) Illustration of structure of double network hydrogel. ii) Pure shear configuration. (b) Log-log plot illustrating the cohesion and adhesion energies, shear modulus as a function of polymer fraction. Sample size N=3.

Consider a steady crack propagation within the damage zone, which resembles a sub-pure shear specimen, the first stiff network is assumed to be completely damaged and the material response is dominated by the 2nd network. By leveraging the energy release rate expression for the pure shear specimen $G_{tip} = Wh$, the critical condition for steady crack propagation $G_{tip} = \Gamma_{Co}$ and the fact that the intrinsic cohesion energy is governed by the 2nd network, we can thus approximate the critical energy release rate to rupture the 2nd network with $\Gamma_{Co} \approx E_2\varepsilon_2^2 h$, where h is the height of the sub-pure shear specimen. On the other hand, the apparent cohesion energy equals the energy per unit length required to expand the damage zone from 0 to h in the undeformed configuration, and thus approximates $G_{apparent} = \Gamma_C \approx \sigma_1 h\varepsilon_2$. Note in the above expression of the apparent and intrinsic cohesion energies, the numerical pre-factors have been dropped. To compare with the experimental results in Figure 4.2, we recast the expression of the cohesion energy into the form $\Gamma_{Co} \approx (E_1\varepsilon_1)/(E_2\varepsilon_2)$. It is reasonable to assume that the critical strain ε_1 corresponding to the yield stress of

the 1st network and the maximum strain at which the same network is completely broken ε_2 have the same scaling with respect to the polymer fraction. Since the 2nd network is essentially polyacrylamide hydrogel as investigated by Li et al. [16], we adopt their finding that the intrinsic cohesion energy Γ_{Co} (fatigue threshold) and the elastic modulus E_2 of the polyacrylamide network share the same scaling with respect to the polymer fraction. Also, we find that the scaling exponent between intrinsic cohesion energy Γ_{Co} and polymer fraction of the tough hydrogel is 0.76 (Figure 4.7), which is close to that between the elastic modulus and polymer fraction of a single network PAAm hydrogel.[16] Thus, we assume the $\Gamma_{Co} \sim E_2$ relationship of tough hydrogels matches that of the PAAm hydrogels. It should be noted that the assumption calls for experimental validation in future work. As the shear modulus of the tough hydrogel $\mu \sim E_1$, we conjecture the cohesion energy and the shear modulus share the same scaling as a function of polymer content, $\Gamma_C \sim \mu$.

To testify the hypothesis, we then characterize the shear modulus μ of the tough adhesive hydrogel using a rheometer (TA HR-2 hybrid rheometer). The swollen hydrogels are gently compressed between parallel plates on the rheometer and subject to a shear strain of 1%. As expected, the shear modulus decreases with the polymer fraction. Remarkably, the result reveals the same scaling relation ($\phi^{2.2}$) between the shear modulus and the polymer fraction (Figure 4.2b). The interpretation of the exponent 2.2 requires further investigation and is out of the scope of this work, as different scaling relations have been reported for hydrogels with different solvent contents and network configuration [25-27]. To further testify this finding with other material systems, we also measured toughness and shear modulus of PNIPAm/Alginate-Ca^{2+} hydrogel at various polymer fractions. The result shows that the scaling for toughness ($\phi^{1.8}$) is close to that for shear modulus

($\phi^{1.6}$) (Figure 4.8). This result confirms the proceeding hypothesis and supports the scaling analysis based on Brown's model for tough hydrogels.

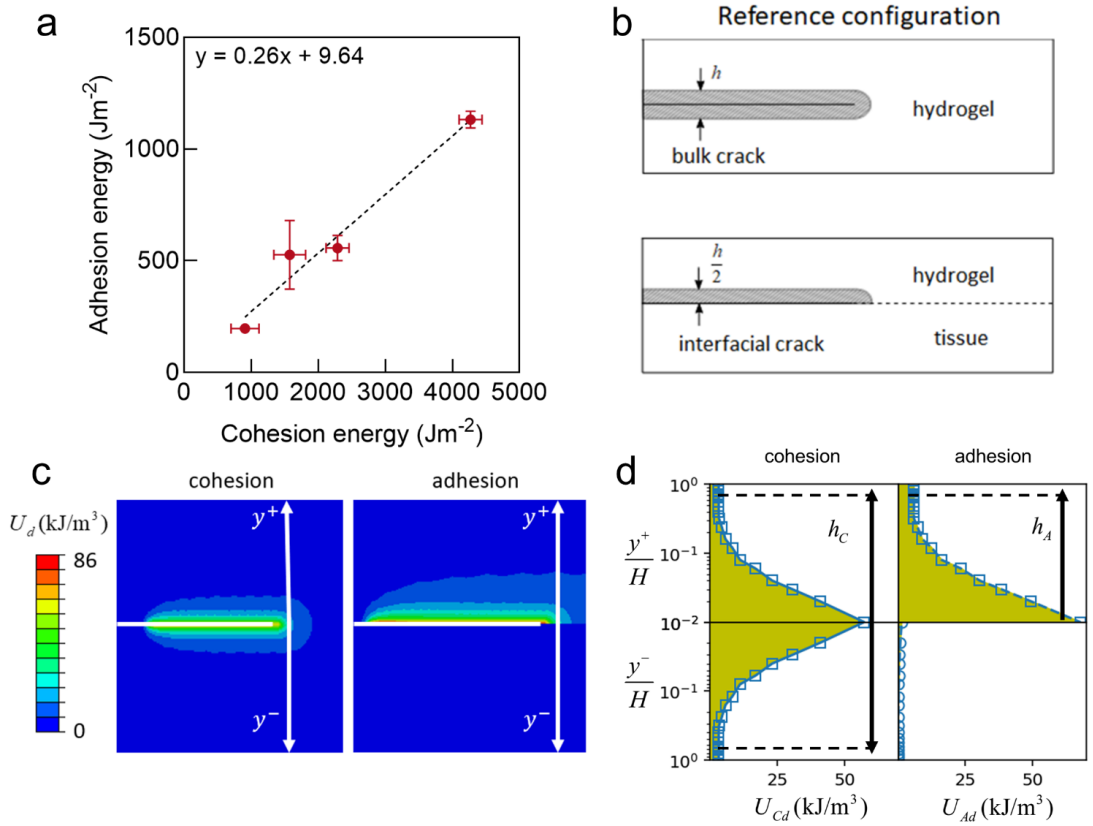

Figure 4.3 Relationship between adhesion energy and cohesion energy. (a) Adhesion energy is about one quarter of cohesion energy. Sample size N=3. (b) Damages zones near a bulk crack and an interfacial crack in the reference configuration of a pure shear specimen during the steady-state crack propagation. (c) A similar plot to (b) with contour plots showing the distribution of the dissipated energy per unit volume U_d when $(S_{\text{interface}})_C / \mu = (S_{\text{interface}})_A / \mu = 12$. The white horizontal lines denote the initial cracks. (d) plots the U_d distribution across the height extracted from the vertical axes in (c). The colored area enclosed by the U_d curve and the y-axis denotes the total dissipated energy in the specimen of height 2H.

We further perform a finite element (FE) study to delineate the correlation between the cohesion and adhesion energies (Figure 4.3). Our experimental results reveal a simple relation between the cohesion energy Γ_C and the adhesion energy Γ_A (Figure 4.3a). By defining an energy enhancement ξ_i due to the bulk energy dissipation of the adhesive hydrogel, the ratio of adhesion and cohesion energies

can be formulated as $\Gamma_A/\Gamma_C = (\Gamma_{Ao}/\Gamma_{Co})(\xi_A/\xi_C)$, where Γ_{io} is the intrinsic energy; the subscription *i* can be *C* or *A*, referring to the cohesion or adhesion case, respectively. Due to the substantial amount of bulk dissipation dominating both the cohesion and adhesion energies, the energy enhancements can be estimated as the dissipated energy normalized by the corresponding intrinsic energy in the adhesion or cohesion case. The decoupling between Γ_{io} and ξ_i has been validated both computationally and analytically [12,13]. We also adopt the FE model by Zhang et al. [13] to simulate the fracture of a pure shear specimen (Figure 4.9a). We find that the energy enhancement ξ_A and ξ_C are indeed independent of Γ_{Ao} andΓ_{Co}, respectively, indicative of the separable dependence of Γ_A/Γ_C on ξ_A/ξ_C and Γ_{Ao}/Γ_{Co} (Figure 4.9c). For the ratio of energy enhancementξ_A/ξ_C, we resort to the FE simulation. For convenience, the intrinsic adhesion energy is set to be equal to the intrinsic cohesion energy in the FE model. We hypothesize that the region of background hysteresis of a crack into the bulk hydrogel (cohesion) is approximately two times that of an interfacial crack between the hydrogel and the skin (adhesion), as the skin is much stiffer thus contributing to negligible dissipation (Figure 4.3b). For steady crack propagation at critical stretch λ_c corresponding to the peak pulling force (Figure 4.9b), the dissipated energy can be determined by integrating the maximum dissipated energy of a unit volume ahead of the crack tip in its loading history U_{id} over the height of the specimen (2H) [12]. With the same intrinsic toughness, we have $\xi_A/\xi_c = \int_{-H}^{H} U_{Ad}(y)dy/\int_{-H}^{H} U_{Cd}(y)dy$. As can be seen in Figure 4.3c, the upper and the lower parts in the cohesion case contribute equally to the total energy dissipation, whereas in the adhesion case only the upper part (adhesive hydrogel) contributes to the energy dissipation and the lower part (tissue) shows negligible energy dissipation. Figure 4.3d plots the energy dissipation distributions across the height in the adhesion and the cohesion cases. Upon the observation, the U_{Ad} and U_{Cd} distributions in the upper parts show a qualitatively similar trend. By adopting a customized definition of the size of the dissipation zone within which 90% of the total energy dissipation in the hydrogel adhesive is manifested, we have $h_A = h_c/2 \approx 0.8H$, which confirms our

hypothesis. The ratio of energy enhancement ξ_A/ξ_C, however, is not exactly $\frac{1}{2}$, likely due to the different crack tip fields in the pure-shear and the interracial crack specimen, which is not the focus of our current study. Furthermore, the above discussion assumes the same bulk-interface coupling in the cohesion and adhesion cases, which can be captured by a dimensionless parameter $(S_{interface})_i/\mu$, where $(S_{interface})_i$ is the cohesive (or adhesive) strength. Specifically, with a higher $(S_{interface})_i/\mu$ value, larger strain is expected in the bulk hydrogel leading to higher dissipated energy [13,14]. To account for different bulk-interface couplings in the adhesion and cohesion cases, we perform additional FE simulations and the results nicely collapse on to a master curve, showing a linear relation between ξ_A/ξ_C and the strength ratio of the adhesion to the cohesion case $(S_{interface})_A/(S_{interface})_C$ (Figure 4.9d). It is reasonable to consider the adhesive strength is smaller than the cohesive strength because otherwise the interfacial crack could propagate into the bulk hydrogel, leading to cohesive failure. The ratio ξ_A/ξ_C approximately varies from 0.4 to 0.7 when $(S_{interface})_A/(S_{interface})_C$ varies from 0.5 to 1. The intrinsic cohesion and adhesion energies of the as-prepared tough hydrogel we measured were 62.7 Jm^{-2} and 26.4 Jm^{-2} (Figure 4.10), respectively, which are consistent with the data reported in literature [28, 29]. Altogether, we calculate the ratio of adhesion and cohesion energies with $\Gamma_A/\Gamma_C = (\Gamma_{Ao}/\Gamma_{Co})(\xi_A/\xi_C)$, yielding a range between 0.16 and 0.3, which is in a good agreement with the experimental result (0.26).

4.3. Conclusion

In summary, we study the coupling between the swelling and fracture behavior of tough adhesive hydrogels. Our results reveal that both cohesion and adhesion energies of tough adhesive hydrogels decay with the swelling process. Thanks to the unique toughening nature of the tough adhesive hydrogel, a simple scaling law exists for the cohesion and adhesion energies as well as the shear modulus to the polymer fraction. The scaling law is corroborated with the scaling analysis and finite element simulation. It is worth noting that the findings are limited to tough

hydrogels whose fracture behavior is governed by background hysteresis. Besides, the scaling value may vary for different types of hydrogels in different solution environments, but our conclusion that $\Gamma_A \sim \Gamma_C \sim \mu$ still retains. This study provides a facile approach to control and predict the fracture properties of hydrogels. It also calls for further development in the scaling theory of tough hydrogels as they gain increasing impacts in broad areas.

4.4. Acknowledgements

Author Contributions

‡ These authors contributed equally. X. N. performed experiments and Z. Y. conducted analysis and simulation. J. L. supervised the project. All authors contributed to and approved the manuscript.

Notes

The authors declare no competing financial interest.

ACKNOWLEDGMENT

This work was supported by Natural Sciences and Engineering Research Council of Canada (Grant RGPIN-2018-04146), Canada Foundation for Innovation (Grant 37719) and Fonds de Recherche du Québec – Nature et technologies (FRQ-NT NC-270740). Z. Y. acknowledged the support from McGill Engineering Doctoral Awards. J. L. acknowledged the support from the Canada Research Chair Program.

4.5. References

1. Li, J.; Celiz, A. D.; Yang, J.; Yang, Q.; Wamala, I.; Whyte, W.; Seo, B. R.; Vasilyev, N. V.; Vlassak, J. J.; Suo, Z.; Mooney, D. J., Tough Adhesives for Diverse Wet Surfaces. *Science.* **2017,** *357* (6349), 378-381.

2. Yuk, H.; Zhang, T.; Lin, S.; Parada, G. A.; Zhao, X., Tough Bonding of Hydrogels to Diverse Non-Porous Surfaces. *Nat. Mater.* **2016,** *15* (2), 190-6.

3. Annabi, N.; Zhang, Y.-N.; Assmann, A.; Sani, E. S.; Cheng, G.; Lassaletta, A. D.; Vegh, A.; Dehghani, B.; Ruiz-Esparza, G. U.; Wang, X., Engineering a Highly Elastic Human Protein–Based Sealant for Surgical Applications. *Sci. Transl. Med.* **2017,** *9* (410), eaai7466.

4. Mehdizadeh, M.; Yang, J., Design Strategies and Applications of Tissue Bioadhesives. *Macromol. Biosci.* **2013,** *13* (3), 271-288.

5. Blacklow, S. O.; Li, J.; Freedman, B. R.; Zeidi, M.; Chen, C.; Mooney, D. J., Bioinspired Mechanically Active Adhesive Dressings to Accelerate Wound Closure. *Sci. Adv.* **2019,** *5* (7), eaaw3963.

6. Kim, Y.; Parada, G. A.; Liu, S.; Zhao, X., Ferromagnetic Soft Continuum Robots. *Sci. Robot.* **2019,** *4* (33), eaax7329.

7. Liu, X.; Liu, J.; Lin, S.; Zhao, X., Hydrogel Machines. *Mater. Today.* **2020,** *36*, 102-124.

8. Seliktar, D., Designing Cell-Compatible Hydrogels for Biomedical Applications. *Science.* **2012,** *336* (6085), 1124-8.

9. Zhang, L.; Cao, Z.; Bai, T.; Carr, L.; Ella-Menye, J.-R.; Irvin, C.; Ratner, B. D.; Jiang, S., Zwitterionic Hydrogels Implanted in Mice Resist the Foreign-Body Reaction. *Nat. Biotechnol.* **2013,** *31* (6), 553-556.

10. Sato, K.; Nakajima, T.; Hisamatsu, T.; Nonoyama, T.; Kurokawa, T.; Gong, J. P., Phase-Separation-Induced Anomalous Stiffening, Toughening, and Self-Healing of Polyacrylamide Gels. *Adv. Mater.* **2015,** *27* (43), 6990-8.

11. Long, R.; Hui, C. Y., Fracture Toughness of Hydrogels: Measurement and Interpretation. *Soft Matter.* **2016,** *12* (39), 8069-8086.

12. Qi, Y.; Caillard, J.; Long, R., Fracture Toughness of Soft Materials with Rate-Independent Hysteresis. *J Mech Phys Solids.* **2018,** *118*, 341-364.

13. Zhang, T.; Lin, S.; Yuk, H.; Zhao, X., Predicting Fracture Energies and Crack-Tip Fields of Soft Tough Materials. *Extreme Mech. Lett.* **2015,** *4*, 1-8.

14. Zhang, T.; Yuk, H.; Lin, S.; Parada, G. A.; Zhao, X., Tough and Tunable Adhesion of Hydrogels: Experiments and Models. *Acta Mech Sin.* **2017,** *33* (3), 543-554.

15. De Gennes, P.-G., *Scaling Concepts in Polymer Physics*. Cornell university press: 1979.

16. Li, Z.; Liu, Z.; Ng, T. Y.; Sharma, P., The Effect of Water Content on the Elastic Modulus and Fracture Energy of Hydrogel. *Extreme Mech. Lett.* **2020,** *35, 100617*.

17. Zhao, X., Designing Toughness and Strength for Soft Materials. *Proc. Natl. Acad. Sci. U. S. A.* **2017,** *114* (31), 8138-8140.

18. Brown, H. R., A Model of the Fracture of Double Network Gels. *Macromolecules.* **2007,** *40* (10), 3815-3818.

19. Sun, J. Y.; Zhao, X.; Illeperuma, W. R.; Chaudhuri, O.; Oh, K. H.; Mooney, D. J.; Vlassak, J. J.; Suo, Z., Highly Stretchable and Tough Hydrogels. *Nature.* **2012,** *489* (7414), 133-6.

20. Yang, J.; Bai, R.; Suo, Z., Topological Adhesion of Wet Materials. *Adv. Mater.* **2018,** *30* (25), e1800671.

21. Bai, R.; Chen, B.; Yang, J.; Suo, Z., Tearing a Hydrogel of Complex Rheology. *J Mech Phys Solids.* **2019,** *125*, 749-761.

22. Gent, A. N., Adhesion and Strength of Viscoelastic Solids. Is There a Relationship between Adhesion and Bulk Properties? *Langmuir.* **1996,** *12* (19), 4492-4496.

23. Yang, J.; Bai, R.; Chen, B.; Suo, Z., Hydrogel Adhesion: A Supramolecular Synergy of Chemistry, Topology, and Mechanics. *Adv. Funct. Mater.* **2019**, 1901693.

24. Duarte, A.; Coelho, J.; Bordado, J.; Cidade, M.; Gil, M., Surgical Adhesives: Systematic Review of the Main Types and Development Forecast. *Prog. Polym. Sci.* **2012,** *37* (8), 1031-1050.

25. Obukhov, S. P.; Rubinstein, M.; Colby, R. H., Network Modulus and Superelasticity. *Macromolecules.* **1994,** *27* (12), 3191-3198.

26. Hoshino, K.-i.; Nakajima, T.; Matsuda, T.; Sakai, T.; Gong, J. P., Network Elasticity of a Model Hydrogel as a Function of Swelling Ratio: From Shrinking to Extreme Swelling States. *Soft Matter.* **2018,** *14* (47), 9693-9701.

27. Sakai, T.; Kurakazu, M.; Akagi, Y.; Shibayama, M.; Chung, U.-i., Effect of Swelling and Deswelling on the Elasticity of Polymer Networks in the Dilute to Semi-Dilute Region. *Soft Matter.* **2012,** *8* (9), 2730-2736.

28. Bai, R.; Yang, Q.; Tang, J.; Morelle, X. P.; Vlassak, J.; Suo, Z., Fatigue Fracture of Tough Hydrogels. *Extreme Mech. Lett.* **2017,** *15*, 91-96.

29. Ni, X.; Chen, C.; Li, J., Interfacial Fatigue Fracture of Tissue Adhesive Hydrogels. *Extreme Mech. Lett.* **2020,** *34*, 100601.

4.6. Supporting Information

4.6.1. Materials

Chemicals used in this work were purchased without further purification. Acrylamide (AAm, monomer), N-isopropylacrylamide (NIPAm, monomer), N'-methylenebis(acrylamide) (MBAA, crosslinker), N,N,N',N'-tetramethylethylenediamine (TEMED, accelerator), ammonium persulfate (APS, initiator), calcium sulfate, N-hydroxysulfosuccinimide (NHS), and 1-ethyl-3-(3-dimethylaminopropyl) carbodiimide (EDC) were purchased from Sigma Aldrich. Alginate (I-1G) was purchased from KIMICA Corporation. Chitosan (deacetylation degree 95%, medium to high molecular weight) was purchased from Xi'an Lyphar Biotech (Shanxi, China). Glass and acrylic sheets were purchased from McMaster-Carr to make reaction molds. Fresh porcine skin was purchased from a local grocery store, then stored in the fridge at -20℃ and thawed at 4℃ before use.

4.6.2. Experimental Methods

Hydrogel adhesive synthesis

PAAm/Alginate hydrogel: Firstly, 6.76 g of AAm monomers and 1.128 g of sodium alginate were dissolved in 50 mL of deionized water. Then, 20 ml of the AAm-alginate solution was mixed with 72 μL of MBAA aqueous solution (0.02 g mL^{-1}) and 16 μL of TEMED in a syringe. Meanwhile, 452 μL of APS solution (0.066 g mL^{-1}) and 382 μL calcium sulfate slurries ($CaSO_4$, 0.207 g mL^{-1}) were drawn into another syringe. Two syringes were connected with a Luer-Lock connector, so the two solutions were syringe-mixed to form a homogeneous solution. The mixture was immediately injected into three groups of molds covered with glass plates and then kept at room temperature for 24 hours to complete the reaction. Group One is a 80 × 20 × 1.5 mm^3 rectangular acrylic mold (for cohesion energy measurement), Group Two is a 80 × 15 × 1.5 mm^3 rectangular mold (for adhesion energy measurement) and Group Three is a circular mold with 15 mm in diameter and 1.5 mm in thickness (for shear modulus measurement).

PNIPAm/Alginate hydrogel: 6 g NIPAm and 1 g alginate power were dissolved in 50 ml DI water. Then we added MBAA (weight ratio to NIPAm is 0.00037), TEMED (weight ratio to NIPAm is 0.0037), APS (weight ratio to NIPAm is 0.000013) and $CaSO_4$ (weight ratio to NIPAm is 0.0022). The precursor solution was mixed and injected into Group One and Three molds covered with glass plates to complete reaction.

Synthesis of tough adhesive hydrogels: One gram of chitosan powder was dissolved into 50 mL of deionized water with 400 μL of acetic acid added for a final pH of 4.5. The mixture was stirred overnight to form a homogenous solution and then kept at 4 ^oC before use. The fresh porcine skin was cut into slices with an area 80 × 15 mm^2. The swollen hydrogels (group Two) were cut into pieces with the same size as that of the skin. Lastly, 30 mg of EDC and 30 mg of NHS were added into 1 mL of the chitosan solution to form an interfacial bonding solution for tissue adhesion, which was subsequently spread onto the epidermal surface of

porcine skin to form adhesion with the swollen hydrogels of varying polymer fractions placed on the top. The length of overlapping joint is 75 mm for adhesion energy measurement. The mold was covered with an acrylic sheet and clamped with binder clips for gentle compression, and then stored in a sealed zip bag at 4 ◦C overnight. Before testing, PET films were glued onto the back of the hydrogel and the skin to constrain their deformation.

Controlled swelling experiments

Before applying the interfacial bonding solution (e.g., chitosan and EDC), performed hydrogels were soaked in a PBS solution of volume 100 times larger than that of the hydrogels. The swelling duration varied between 0, 0.5, 1, 2, 3, 4, 5 and 6 hours; the 0-hour condition refers to as-prepared hydrogels without swelling. To ensure homogenous water distribution within the hydrogel matrix, the swollen gels were placed in a sealed bag for additional 12 hours. Considering the diffusivity of small molecules (e.g., water molecules and ions) in water $\mathrm{D} \approx 10^{-10}\,\mathrm{m^2 s^{-1}}$ and half of the thickness of swollen hydrogel is 1 mm, we estimate the time period from taking hydrogel out of water to reaching homogeneity to be $\tau = L^2 / D \approx 10^4\,\mathrm{s} \approx 3\ \mathrm{hours}$. Thus, 12 hours are enough for homogenous water distribution process.

The polymer content of hydrogels was measured after lyophilization. The as-prepared hydrogel samples were placed in a freezer (-20 ℃) for 5 hours and then moved to a deep freezer of -80 ℃ for 12 hours. The frozen samples were transferred into a freeze dryer immediately and dehydrated for 48 hours. The weight of dry samples was measured and denoted by m_{polymer} . The weight of hydrogel samples with various water content was measured and denoted by m_{gel} . The density of dry polymer ρ_{polymer} is taken to be the weighted average of those of alginate and acrylamide, which is 1.172 gcm^{-3}. The density of gel ρ_{gel} is approximately 1 gcm^{-3}. The polymer fraction is defined as the following:

$$\phi = \frac{V_{\text{polymer}}}{V_{\text{gel}}} = \frac{m_{\text{polymer}} / \rho_{\text{polymer}}}{m_{\text{gel}} / \rho_{\text{gel}}}.$$

Mechanical testing

A tearing test was adopted to measure the toughness of hydrogel. After swelling, rectangular hydrogel samples with various water content (Group One) were cut to be 20 mm in width and 80 mm in length. The thickness of each sample was measured and recorded with a vernier caliper. Then PET films with 10 mm width and 80 mm length were glued on the top and bottom surfaces of the hydrogel covering half of each surface of the sample using the Krazy glue with no observable gap in the midline. Afterwards, an initial crack of 15 mm was cut along the midline of the hydrogel using a razor blade, forming two arms of 10 mm width and 15 mm length. Two arms were stretched by grips of a tensile testing machine (Instron 5965) with a 1 kN load cell. During the tearing test, the machine maintained a constant loading speed (0.5 mm s^{-1}) and recorded the force.

180-degree peeling test was adopted to measure the adhesion energy of tough adhesive hydrogels (TA). After specimen prepared, free arms of TA and the substrate were attached to plastic sheets stretched by machine grips. An Instron machine (Model 5965 with load cell of 1 kN) was used to apply unidirectional tension, while recording the force and the extension. The loading speed was kept constant at 0.5 mm s^{-1}.

Rheological test was adopted to measure the shear modulus of hydrogel. After swelling, circular hydrogel samples with various water content were cut to be 20 mm in diameter. Rheological measurements were carried out using TA-Discovery HR-2 rheometer equipped with a 20 mm steel parallel plate at 25 ℃. Frequency sweeps were carried out at 1% strain from 0.05 Hz to 1 Hz, while recording storage modulus. The first three values of storage modulus were used to extrapolate the value at f=0 Hz, which is considered as shear modulus.

Pure-shear fatigue test was adopted to measure the intrinsic cohesion energy of hydrogel. Following reported procedures[1, 2], a hydrogel sample was cut with a 20 mm crack at middle, and then stretched by a cyclic loading at various maximum stretch. The loading frequency was kept as 0.5 Hz. During test, the whole sample was put inside a biobath with water droplets spread on the inner surface to minimize dehydration. A digital camera recorded crack length growth. The crack growth speed dc/dN was plotted as a function of energy release rate. By linear extrapolation, the interception with x-axis gives intrinsic cohesion energy Γ_{Co}.

180-degree peeling fatigue test was adopted to measure the intrinsic adhesion energy of hydrogel. Following reported procedures[2], we applied cyclic peeling force with fixed amplitude F. The interfacial crack length c was recorded from Instron tensile machine as together with cycle number N. The applied energy release rate was $G = 2F / w$. Then interfacial crack growth speed dc/dN was plotted as a function of energy release rate *G*. By linear extrapolation, the interception with x-axis gives intrinsic adhesion energy Γ_{Ao}.

4.6.3. Finite Element Simulation

The commercial package ABAQUS (2020, Simulia) was used for the finite element analysis. The FE model developed by Zhang et al.[3] was adopted in the current study, which has been validated in a previous work[4]. Briefly, a crack is introduced to a pure shear specimen, shown in Figure 4.9a, with the top boundary subjected to a progressively increased displacement and the bottom boundary constrained. The model is based on the plane-stress assumption (the in-plane dimensions are much larger than the out-of-plane dimension) and the hydrogel is modelled using the combined Ogden and the modified Ogden-Roxburgh model: $W = \eta\widehat{W} + \phi(\eta)$, where η is the damage variable (η = 1 and 0 represents the material in its undamaged and completely damaged state, respectively); $\widehat{W} = \frac{2\mu}{\alpha^2}(\lambda_1^\alpha + \lambda_2^\alpha + \lambda_3^\alpha - 3)$ is the free energy function without energy dissipation; μ and α are the Ogden

coefficients and $\lambda_i, i=1,2,3$ is the i^{th} principle stretch; $\phi(\eta)=\int_1^{\eta}\left[(m+\beta W^m)\text{erf}^{-1}(r(1-\eta))-W^m\right]d\eta$ is the damage function; W^m the maximum strain energy density before unloading erf the error function. The Mullin's parameters r, m, β along with the Ogden coefficients for the hydrogel and skin are shown in Table S1. The parameters for the hydrogel are obtained by performing a series of cyclic loading tests using the pure specimen; those for the skin are obtained by fitting the material model mentioned above to the results reported in an experimental literature[5]. A qualitative loading-unloading curve of a material point near the crack tip is shown in the upper inset of Figure 4.9a. The area enclosed by the curve represents the energy dissipation density U_d (highlighted in yellow)。

Table 4.1 Ogden and Mullin's coefficients for Skin and Gel

	Ogden		**Mullins Parameters**		
	$\mu(\mathbf{kPa})$	α	r	$m(\text{kJm}^{-3})$	β
Skin	272.2	22.25	1.255	1.012	0.720
Gel	10.81	2	1.516	4.274	0.1

The upper and lower parts are bonded using a layer of cohesive elements, which is characterized by a triangular traction-separation law [lower inset of Figure 4.9a]. $\delta_{interface}$ and $S_{interface}$ are the maximum displacement and strength, respectively, and the area under the curve is the intrinsic work of adhesion Γ_0 (highlighted in yellow). The cohesive elements are assumed to be crack mode-independent and the damage initiation is governed by the quadratic nominal stress criterion $(\frac{t_n}{S_{interface}})^2+(\frac{t_s}{S_{interface}})^2=1$, where t_n and t_s are the cohesive tractions in the directions normal and tangential to the interface, respectively.

4.6.4. Cohesion and Adhesion Failure

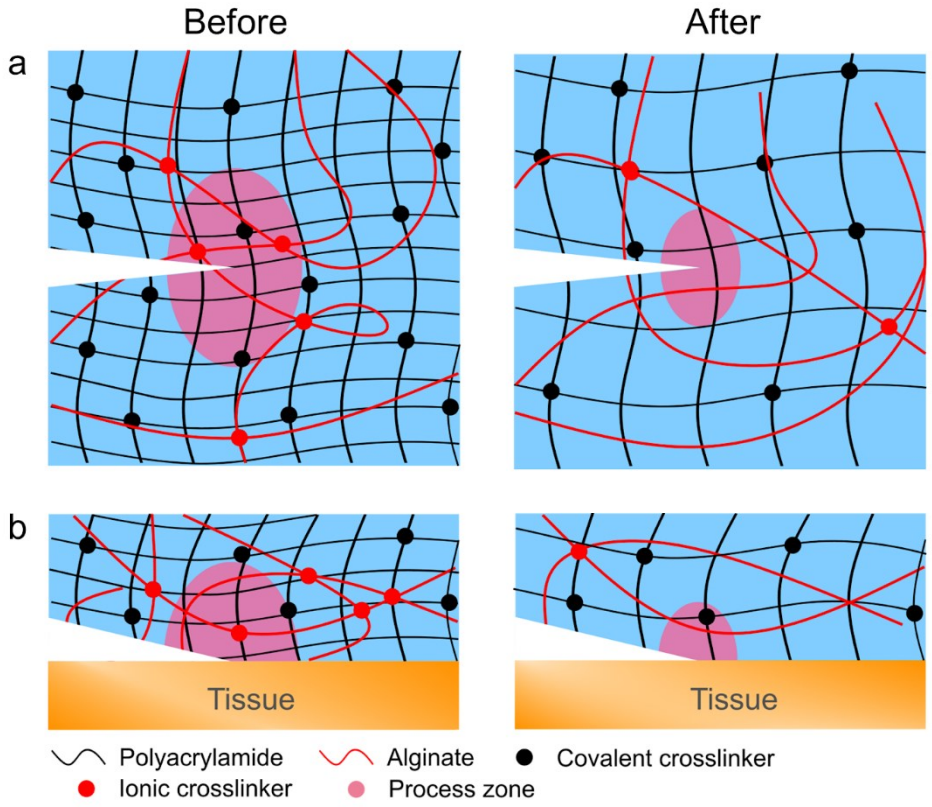

Figure 4.4 Schematic illustration of cohesion (a) and adhesion (b) failure of tissue adhesive hydrogels before and after swelling. Swelling reduces the polymer fraction and the concentration of bound Ca^{2+}, lowering the energy dissipation capacity of the hydrogel matrix.

4.6.5. Polymer Fraction Decreasing as Swelling

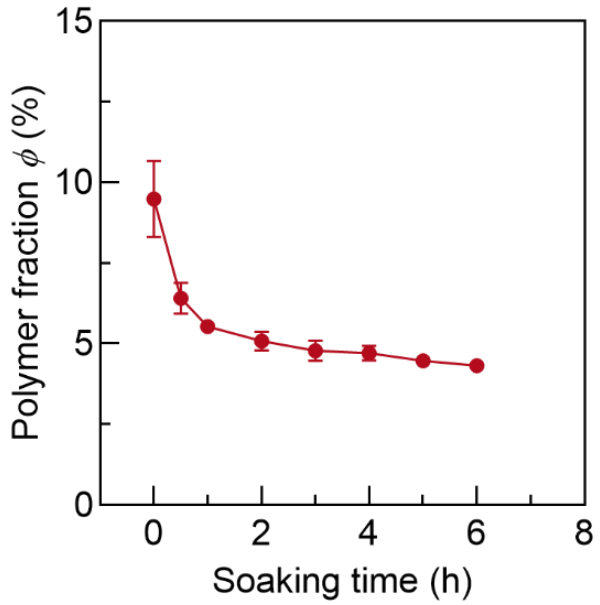

Figure 4.5. Polymer fraction decreases with soaking time.

4.6.6. One Cycle Loading Curve of Tough Hydrogel

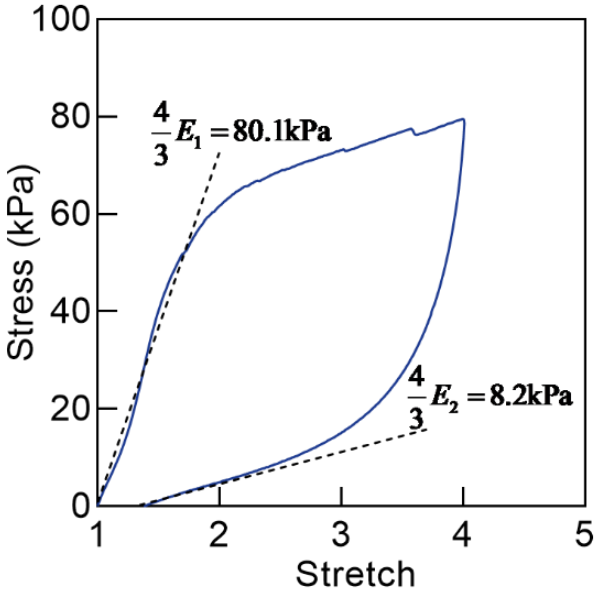

Figure 4.6 The stress-stretch curve of tough hydrogel under one cycle loading in a pure shear specimen. The elastic modulus at loading stage E_1 is one order of magnitude larger than that at unloading stage E_2.

4.6.7. Intrinsic Cohesion Energy vs. Polymer Fraction

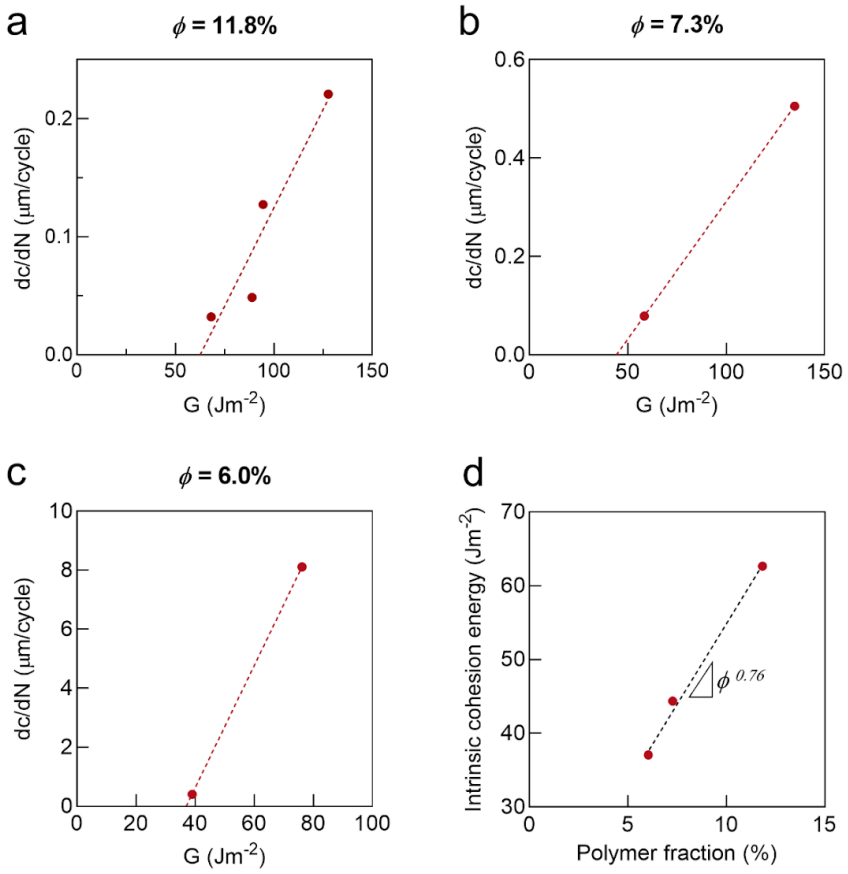

Figure 4.7 The relationship between intrinsic cohesion energy and polymer fraction. (a)-(c) The crack growth speed dc/dN is plotted as a function of energy release rate G at various polymer fraction to obtain intrinsic cohesion energy Γ_{Co}. (d) The scaling exponent between intrinsic cohesion energy and polymer fraction is 0.76.

4.6.8. A Scaling Law in PNIPAm/Alginate Hydrogel

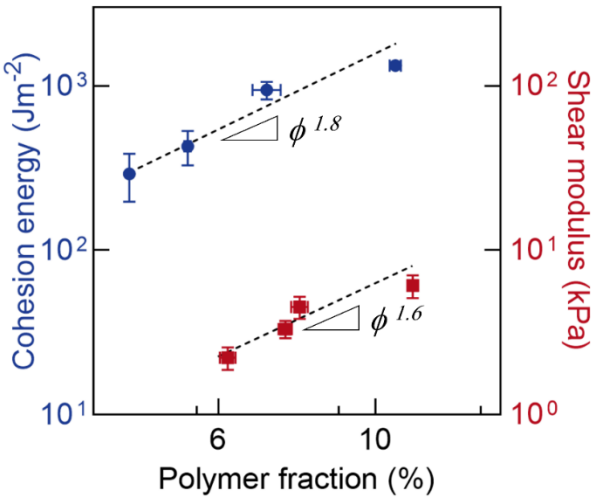

Figure 4.8 Log-log plot of cohesion energy and shear modulus as a function of polymer fraction for PNIPAm/Alginate hydrogels.

4.6.9. FEM of Cohesion and Adhesion Failure

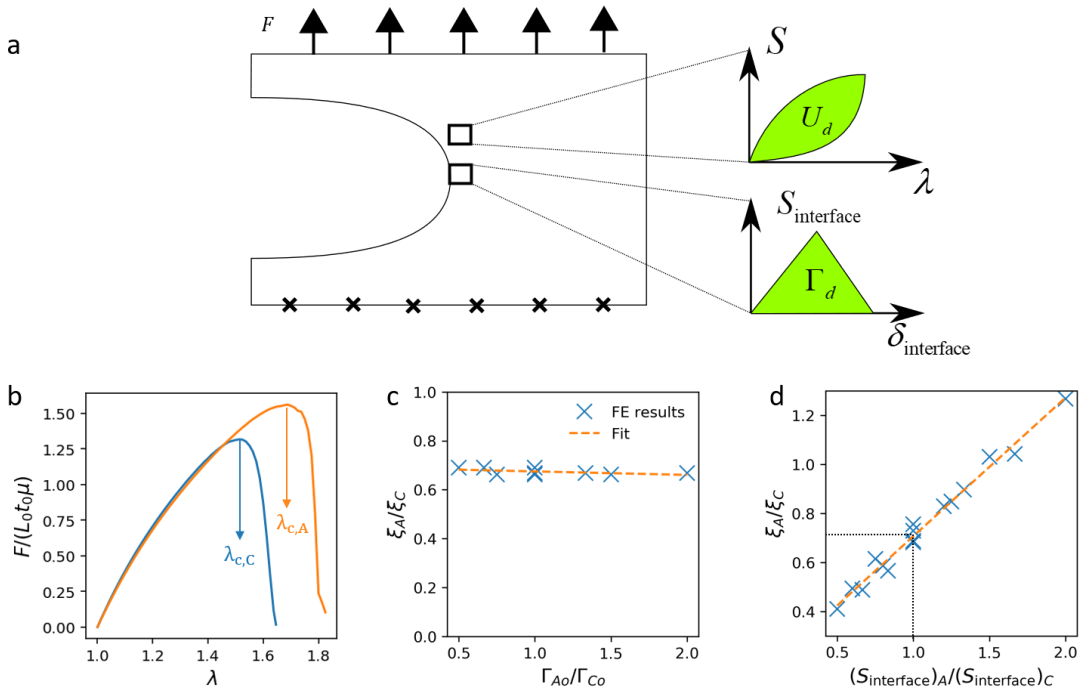

Figure 4.9 Finite element simulation of the cohesion and adhesion failure. (a) Pure-shear specimen in the deformed configuration. The specimen has an initial length of L_0 and an out-of-plane thickness t_0. The upper-right inset shows the nominal stress-stretch curve of a bulk material along the loading and unloading path; the lower-right inset shows

the traction-separation low for the cohesive elements on the interface. (b) Normalized pulling force plotted against the stretch ratio for the cohesion and the adhesion cases with $(S_{interface}/\mu)_A = (S_{interface}/\mu)_C = 12$. (c) Ratio of the enhancement factors ξ_A/ξ_C plotted against Γ_{Ao}/Γ_{Co}. Data are obtained from simulations with different Γ_{Ao} and Γ_{Co} varying from 60 to 120 J/m^2 and $(S_{interface}/\mu)_A = (S_{interface}/\mu)_C = 12$. (d) Ratio of the enhancement factors ξ_A/ξ_C as a function of $(S_{interface})_A/(S_{interface})_C$. Data are obtained from simulations with different $(S_{interface})_A$ and $(S_{interface})_C$ varying from 60 to 120 kPa.

4.6.10. Intrinsic Cohesion Energy and Intrinsic Adhesion Energy

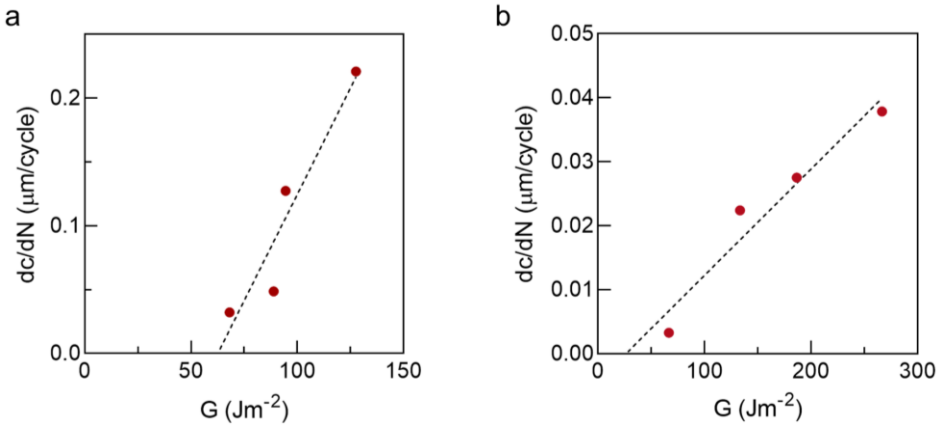

Figure 4.10 Intrinsic cohesion energy (a) and intrinsic adhesion energy (b) are measure from fatigue tests. (a) crack growth speed dc/dN is plotted as a function of energy release rate. A threshold gives $\Gamma_{Co} = 62.7\, Jm^{-2}$. (b) $\Gamma_{Ao} = 26.4\, Jm^{-2}$.

References

1. Bai, R.; Yang, Q.; Tang, J.; Morelle, X. P.; Vlassak, J.; Suo, Z., Fatigue Fracture of Tough Hydrogels. *Extreme Mech. Lett.* **2017,** *15*, 91-96.

2. Liu, J.; Lin, S.; Liu, X.; Qin, Z.; Yang, Y.; Zang, J.; Zhao, X., Fatigue-Resistant Adhesion of Hydrogels. *Nat. Commun.* **2020,** *11* (1), 1071.

3. Zhang, T.; Yuk, H.; Lin, S.; Parada, G. A.; Zhao, X., Tough and Tunable Adhesion of Hydrogels: Experiments and Models. *Acta Mech. Sin.* **2017,** *33* (3), 543-554.

4. Zhang, T.; Lin, S.; Yuk, H.; Zhao, X., Predicting Fracture Energies and Crack-Tip Fields of Soft Tough Materials. *Extreme Mech. Lett.* **2015,** *4*, 1-8.

5. Munoz, M.; Bea, J.; Rodríguez, J.; Ochoa, I.; Grasa, J.; del Palomar, A. P.; Zaragoza, P.; Osta, R.; Doblaré, M., An Experimental Study of the Mouse Skin Behaviour: Damage and Inelastic Aspects. *J. Biomech.* **2008,** *41* (1), 93-99.

Chapter 5. Conclusion and Recommendation

5.1. Conclusion

In this thesis, we studied the fracture behaviors of tough adhesive hydrogels under cyclic loading and in swelling conditions, revealing the fatigue fracture and the correlation among modulus, toughness and adhesion energy of tough adhesive hydrogels.

First, we systematically studied the interfacial fracture of tough adhesive hydrogels under three kinds of loading (monotonic, static and cyclic loads) and observed two fracture behaviors (fast fracture and fatigue fracture). Furthermore, we investigated the fatigue fracture by applying different maximum stretch. The interfacial fatigue fracture threshold was found to be 24 Jm^{-2} through measuring the crack growth rate under different loading. We also compared the fatigue threshold of tough adhesive hydrogel with that of bulk hydrogel, showing the interfacial fatigue threshold is lower than the fatigue threshold of bulk hydrogel.

Moreover, we studied the effect of swelling on the fracture behaviors of tough adhesive hydrogels. The results show that fracture properties (cohesion and adhesion energies) of tough adhesive hydrogels deteriorate as swelling. We discovered a scaling law of cohesion energy, adhesion energy and shear modulus to the polymer fraction, which is analyzed by scaling theories and finite element simulation.

Our studies reveal fracture behaviors of tough adhesive hydrogels under common loading conditions and found a simple way to control fracture properties of hydrogels. These findings would be helpful to promote study on the fracture of hydrogels and develop next-generation tissue adhesives.

5.2. Recommendations

Recent years, hydrogel adhesives have rapidly evolved. Many approaches were proposed to achieve strong hydrogel adhesion. However, some challenges still remain to be solved. In the following, we recommend several future research directions.

Our results in Chapter 3 show interfacial fatigue fracture is prone to happen for tough adhesive hydrogels under cyclic loading, despite the measured high adhesion energy under monotonic loading. The underlying reason could be linked with the bridging polymer, which is likely mechanically weaker than the polymer networks in hydrogel matrix. Thus, future research could include developing fatigue-resistant tissue adhesive hydrogels. Based on previous studies about fatigue of hydrogels [11-13, 94, 96], a fundamental principle is recognized that tougheners greatly enhance the toughness, but contribute negligibly to the fatigue threshold. Currently, there are some strategies that could achieve high fatigue threshold of hydrogel adhesion, for example, using extremely long polymer chains [108] or nanocrystalline domains [67]. However, these strategies can not be directly applied to tissue adhesion due to the harsh preparation condition and toxic precursors. According to the progress in fatigue-resistant hydrogels [109-111], cracks are required to be pinned or deflected to resist fatigue failure. Fiber reinforcement and nanocrystalline formed in a biocompatible manner are possible choices.

In Chapter 4, we discovered and established a simple universal scaling law for fracture properties and elastic modulus of tough hydrogels as a function of polymer fraction. But the fundamental mechanism underlying this scaling law is still unclear and calls for further investigation, as well as its applicability to other hydrogel systems. Because fracture behaviors of tough hydrogels involve complex energy dissipation mechanism, currently there is no scaling theory that can capture such relation. In the future, we plan to investigate the physical mechanism behind the scaling law. Even though it is already known swelling would greatly weakens

mechanical properties of hydrogels, the effect of dehydration is still lack of investigation. Previous study shows that the scaling exponent for PAAm hydrogel is different in swelling process and dehydration [107], indicating swelling and dehydration influence hydrogels in a different manner. Because hydrogels easily lose water in open air, investigating the effect of dehydration on mechanical properties is critical to exploit hydrogels in real applications.

With increasing use of tough adhesive hydrogels in broad applications, the study of the fracture behaviors of these hydrogels under various application setting and loading conditions is critical both from the fundamental and practical perspectives. This research area remains in a nascent stage but is expected to grow in importance in years to come.

References

1. Artzi, N., Sticking with the pattern for a safer glue. *Sci. Transl. Med*., 2013. **5**(205): p. 205ec161-205ec161.
2. Nam, S. and D. Mooney, Polymeric tissue adhesives. *Chem. Rev.*, 2021.
3. Taboada, G.M., et al., Overcoming the translational barriers of tissue adhesives. *Nat. Rev. Mater.*, 2020. **5**(4): p. 310-329.
4. Li, J., et al., Tough adhesives for diverse wet surfaces. *Science*, 2017. **357**(6349): p. 378-381.
5. Yuk, H., et al., Tough bonding of hydrogels to diverse non-porous surfaces. *Nat. Mater.*, 2016. **15**(2): p. 190-6.
6. Gao, Y., K. Wu, and Z. Suo, Photodetachable adhesion. *Adv. Mater.*, 2019. **31**(6): p. e1806948.
7. Yang, H., et al., Strong and degradable adhesion of hydrogels. *ACS Appl. Bio Mater.*, 2019.
8. Blacklow, S.O., et al., Bioinspired mechanically active adhesive dressings to accelerate wound closure. *Sci. Adv.*, 2019. **5**(7): p. eaaw3963.
9. Levine, H.J., Rest heart rate and life expectancy. *J Am Coll Cardiol*, 1997. **30**(4): p. 1104-6.
10. Witvrouw, E., et al., The role of stretching in tendon injuries. *Br J Sports Med*, 2007. **41**(4): p. 224-6.
11. Bai, R., et al., Fatigue fracture of self-recovery hydrogels. *ACS Macro Lett.*, 2018. **7**(3): p. 312-317.
12. Bai, R., et al., Fatigue fracture of tough hydrogels. *Extreme Mech. Lett.*, 2017. **15**: p. 91-96.
13. Tang, J., et al., Fatigue fracture of hydrogels. *Extreme Mech. Lett.*, 2017. **10**: p. 24-31.
14. Sato, K., et al., Phase-separation-induced anomalous stiffening, toughening, and self-healing of polyacrylamide gels. *Adv. Mater.*, 2015. **27**(43): p. 6990-8.
15. Sakai, T., et al., Effect of swelling and deswelling on the elasticity of polymer networks in the dilute to semi-dilute region. *Soft Matter*, 2012. **8**(9): p. 2730-2736.
16. Samanta, H.S. and S.K. Ray, Synthesis, characterization, swelling and drug release behavior of semi-interpenetrating network hydrogels of sodium alginate and polyacrylamide. *Carbohydr. Polym.*, 2014. **99**: p. 666-678.
17. Tanaka, T. and D.J. Fillmore, Kinetics of swelling of gels. *J. Chem. Phys*., 1979. **70**(3): p. 1214-1218.
18. Lee, K.Y. and D.J. Mooney, Hydrogels for tissue engineering. *Chem. Rev.*, 2001. **101**(7): p. 1869-1880.
19. Nguyen, K.T. and J.L. West, Photopolymerizable hydrogels for tissue engineering applications. *Biomaterials*, 2002. **23**(22): p. 4307-14.
20. Peppas, N.A., et al., Hydrogels in pharmaceutical formulations. *Eur J Pharm Biopharm*, 2000. **50**(1): p. 27-46.
21. Qiu, Y. and K. Park, Environment-sensitive hydrogels for drug delivery. *Adv. Drug. Deliv. Rev.*, 2001. **53**(3): p. 321-39.

22. Ghobril, C. and M.W. Grinstaff, The chemistry and engineering of polymeric hydrogel adhesives for wound closure: A tutorial. *Chem. Soc. Rev.*, 2015. **44**(7): p. 1820-35.
23. Nguyen, Q.V., et al., Injectable polymeric hydrogels for the delivery of therapeutic agents: A review. *Eur. Polym. J.*, 2015. **72**: p. 602-619.
24. Discher, D.E., P. Janmey, and Y.-l. Wang, Tissue cells feel and respond to the stiffness of their substrate. *Science*, 2005. **310**(5751): p. 1139-1143.
25. Engler, A.J., et al., Matrix elasticity directs stem cell lineage specification. *Cell*, 2006. **126**(4): p. 677-689.
26. Kopecek, J., Hydrogels from soft contact lenses and implants to self-assembled nanomaterials. *J. Polym. Sci. A. Polym. Chem.*, 2009. **47**(22): p. 5929-5946.
27. Dong, L., et al., Adaptive liquid microlenses activated by stimuli-responsive hydrogels. *Nature*, 2006. **442**(7102): p. 551-4.
28. Holtz, J.H. and S.A. Asher, Polymerized colloidal crystal hydrogel films as intelligent chemical sensing materials. *Nature*, 1997. **389**(6653): p. 829-832.
29. Yuk, H., et al., Hydraulic hydrogel actuators and robots optically and sonically camouflaged in water. *Nat. Commun.*, 2017. **8**: p. 14230.
30. Li, T., et al., Fast-moving soft electronic fish. *Sci. Adv.*, 2017. **3**(4): p. e1602045.
31. Keplinger, C., et al., Stretchable, transparent, ionic conductors. *Science*, 2013. **341**(6149): p. 984-7.
32. Kim, C.C., et al., Highly stretchable, transparent ionic touch panel. *Science*, 2016. **353**(6300): p. 682-7.
33. Bonn, D., et al., Delayed fracture of an inhomogeneous soft solid. *Science*, 1998. **280**(5361): p. 265-267.
34. Taylor, D., et al., The fracture toughness of soft tissues. *J Mech Behav Biomed Mater*, 2012. **6**: p. 139-47.
35. Tavichakorntrakool, R., et al., K^+, Na^+, Mg^{2+}, Ca^{2+}, and water contents in human skeletal muscle: Correlations among these monovalent and divalent cations and their alterations in K^+-depleted subjects. *Transl. Res.*, 2007. **150**(6): p. 357-66.
36. Utech, S. and A.R. Boccaccini, A review of hydrogel-based composites for biomedical applications: Enhancement of hydrogel properties by addition of rigid inorganic fillers. *J. Mater. Sci.*, 2016. **51**(1): p. 271-310.
37. Gong, J.P., et al., Double-network hydrogels with extremely high mechanical strength. *Adv. Mater.*, 2003. **15**(14): p. 1155-1158.
38. Sun, J.Y., et al., Highly stretchable and tough hydrogels. *Nature*, 2012. **489**(7414): p. 133-6.
39. Lee, C.H., et al., Characterization of heterogeneous polyacrylamide hydrogels by tracking of single quantum dots. *Macromolecules*, 2014. **47**(2): p. 741-749.
40. Lin, W.-C., et al., Large strain and fracture properties of poly(dimethylacrylamide)/silica hybrid hydrogels. *Macromolecules*, 2010. **43**(5): p. 2554-2563.

41. Gong, J.P. and Y. Osada, *Soft and wet materials: From hydrogels to biotissues*. *High solid dispersions*, 2010. p. 203-246.
42. Zheng, S.Y., et al., Metal-coordination complexes mediated physical hydrogels with high toughness, stick–slip tearing behavior, and good processability. *Macromolecules*, 2016. **49**(24): p. 9637-9646.
43. Liao, I.-C., et al., Composite three-dimensional woven scaffolds with interpenetrating network hydrogels to create functional synthetic articular cartilage. *Adv. Funct. Mater.*, 2013. **23**(47): p. 5833-5839.
44. Sakai, T., et al., Design and fabrication of a high-strength hydrogel with ideally homogeneous network structure from tetrahedron-like macromonomers. *Macromolecules*, 2008. **41**(14): p. 5379-5384.
45. Akagi, Y., et al., Evaluation of topological defects in tetra-peg gels. *Macromolecules*, 2010. **43**(1): p. 488-493.
46. Gong, J.P., Why are double network hydrogels so tough? *Soft Matter*, 2010. **6**(12): p. 2583-2590.
47. Tanaka, Y., A local damage model for anomalous high toughness of double-network gels. *Europhys. Lett*, 2007. **78**(5): p. 56005.
48. Darnell, M.C., et al., Performance and biocompatibility of extremely tough alginate/polyacrylamide hydrogels. *Biomaterials*, 2013. **34**(33): p. 8042-8048.
49. Hur, J., et al., Polypyrrole/agarose-based electronically conductive and reversibly restorable hydrogel. *ACS Nano*, 2014. **8**(10): p. 10066-10076.
50. Lin, S., et al., Stretchable hydrogel electronics and devices. *Adv. Mater.*, 2016. **28**(22): p. 4497-4505.
51. Wang, M.X., et al., Rapid self-recoverable hydrogels with high toughness and excellent conductivity. *ACS Appl. Mater. Interfaces*, 2018. **10**(31): p. 26610-26617.
52. Haraguchi, K., Nanocomposite hydrogels. *Curr. Opin. Solid State Mater. Sci.*, 2007. **11**(3): p. 47-54.
53. Haraguchi, K. and T. Takehisa, Nanocomposite hydrogels: A unique organic-inorganic network structure with extraordinary mechanical, optical, and swelling/de-swelling properties. *Adv. Mater.*, 2002. **14**(16): p. 1120-1124.
54. Zhang, Y.-Z., et al., Mxenes stretch hydrogel sensor performance to new limits. *Sci. Adv.*, 2018. **4**(6): p. eaat0098.
55. Li, J., et al., Tough composite hydrogels with high loading and local release of biological drugs. *Adv. Healthc. Mater.*, 2018. **7**(9): p. 1701393.
56. Yuk, H., et al., Dry double-sided tape for adhesion of wet tissues and devices. *Nature*, 2019. **575**(7781): p. 169-174.
57. Prausnitz, M.R. and R. Langer, Transdermal drug delivery. *Nat. Biotechnol.*, 2008. **26**(11): p. 1261-1268.
58. Jung, H., et al., Adhesive hydrogel patch with enhanced strength and adhesiveness to skin for transdermal drug delivery. *Adv. Funct. Mater.*, 2020. **30**(42): p. 2004407.

59. Sarwar, M.S., et al., Bend, stretch, and touch: Locating a finger on an actively deformed transparent sensor array. *Sci. Adv.*, 2017. **3**(3): p. e1602200.
60. Annabi, N., et al., Elastic sealants for surgical applications. *Eur. J. Pharm. Biopharm.*, 2015. **95**: p. 27-39.
61. Yang, C. and Z. Suo, Hydrogel ionotronics. *Nat. Rev. Mater.*, 2018. **3**(6): p. 125-142.
62. Singer, A.J., J.V. Quinn, and J.E. Hollander, The cyanoacrylate topical skin adhesives. *Am. J. Emerg. Med.*, 2008. **26**(4): p. 490-496.
63. Takahashi, R., et al., Tough particle-based double network hydrogels for functional solid surface coatings. *Adv. Mater. Interfaces*, 2018. **5**(23): p. 1801018.
64. Wirthl, D., et al., Instant tough bonding of hydrogels for soft machines and electronics. *Sci. Adv.*, 2017. **3**(6): p. e1700053.
65. Rose, S., et al., Nanoparticle solutions as adhesives for gels and biological tissues. *Nature*, 2014. **505**(7483): p. 382-385.
66. Zhao, X., et al., Soft materials by design: Unconventional polymer networks give extreme properties. *Chem. Rev.*, 2021. **121**(8): p. 4309-4372.
67. Liu, J., et al., Fatigue-resistant adhesion of hydrogels. *Nat. Commun.*, 2020. **11**(1): p. 1071.
68. Rose, S., et al., Nanoparticle solutions as adhesives for gels and biological tissues. *Nature*, 2014. **505**(7483): p. 382.
69. Yuk, H., et al., Skin-inspired hydrogel-elastomer hybrids with robust interfaces and functional microstructures. *Nat. Commun.*, 2016. **7**: p. 12028.
70. Liu, Q., et al., Bonding dissimilar polymer networks in various manufacturing processes. *Nat. Commun.*, 2018. **9**(1): p. 846.
71. Serban, M.A., B. Panilaitis, and D.L. Kaplan, Silk fibroin and polyethylene glycol-based biocompatible tissue adhesives. *J. Biomed. Mater. Res. A*, 2011. **98A**(4): p. 567-575.
72. Chen, B., et al., Molecular staples for tough and stretchable adhesion in integrated soft materials. *Adv. Healthc. Mater.*, 2019. **8**(19): p. e1900810.
73. Wang, Y., et al., Instant, tough, noncovalent adhesion. *ACS Appl. Mater. Interfaces*, 2019. **11**(43): p. 40749-40757.
74. Moretti, M., et al., Structural characterization and reliable biomechanical assessment of integrative cartilage repair. *J. Biomech.*, 2005. **38**(9): p. 1846-54.
75. Bobyn, J.D., et al., Effect of pore size on the peel strength of attachment of fibrous tissue to porous-surfaced implants. *J. Biomed. Mater. Res.*, 1982. **16**(5): p. 571-84.
76. Jeon, E.Y., et al., Bio-inspired swellable hydrogel-forming double-layered adhesive microneedle protein patch for regenerative internal/external surgical closure. *Biomaterials*, 2019. **222**: p. 119439.
77. Rivlin, R. and A.G. Thomas, Rupture of rubber. I. Characteristic energy for tearing. *J. Polym. Sci.*, 1953. **10**(3): p. 291-318.
78. Baumberger, T., C. Caroli, and D. Martina, Solvent control of crack dynamics in a reversible hydrogel. *Nat. Mater.*, 2006. **5**(7): p. 552-555.

79. Seitz, M.E., et al., Fracture and large strain behavior of self-assembled triblock copolymer gels. *Soft Matter*, 2009. **5**(2): p. 447-456.
80. Greensmith, H., Rupture of rubber. X. The change in stored energy on making a small cut in a test piece held in simple extension. *J. Appl. Polym. Sci.*, 1963. **7**(3): p. 993-1002.
81. Gent, A.N., Adhesion and strength of viscoelastic solids. Is there a relationship between adhesion and bulk properties?. *Langmuir*, 1996. **12**(19): p. 4492-4496.
82. Keller, M.W., S.R. White, and N.R. Sottos, A self-healing poly(dimethyl siloxane) elastomer. *Adv. Funct. Mater.*, 2007. **17**(14): p. 2399-2404.
83. King, D.R., et al., Extremely tough composites from fabric reinforced polyampholyte hydrogels. *Mater. Horiz.*, 2015. **2**(6): p. 584-591.
84. Wang, Y., T. Yin, and Z. Suo, Polyacrylamide hydrogels. Iii. Lap shear and peel. *J. Mech. Phys. Solids*, 2021. **150**: p. 104348.
85. Wang, Y., et al., Strength and toughness of adhesion of soft materials measured in lap shear. *J. Mech. Phys. Solids*, 2020. **143**: p. 103988.
86. Wang, Y., et al., Lap shear of a soft and elastic adhesive. *Mech. Mater*, 2021. **158**: p. 103845.
87. Kendall, Crack propagation in lap shear joints. *J. Phys. D: Appl. Phys*, 1975. **8**(5): p. 512.
88. Council, P.S.T., Test methods for pressure sensitive adhesive tapes. 2000.
89. Evans, A.G. and S.M. Wiederhorn, Proof testing of ceramic materials—an analytical basis for failure prediction. *Int. J. Fract.*, 1974. **10**(3): p. 379-392.
90. Fleck, N.A., K.J. Kang, and M.F. Ashby, Overview no. 112: The cyclic properties of engineering materials. *Acta Metall. Mater.*, 1994. **42**(2): p. 365-381.
91. Mars, W.V. and A. Fatemi, Factors that affect the fatigue life of rubber: A literature survey. *Rubber Chem. Technol.*, 2004. **77**(3): p. 391-412.
92. Ritchie, R.O., Mechanisms of fatigue crack propagation in metals, ceramics and composites: Role of crack tip shielding. *Mater. Sci. Eng. A*, 1988. **103**(1): p. 15-28.
93. Li, X., et al., Mesoscale bicontinuous networks in self-healing hydrogels delay fatigue fracture. *Proc. Natl. Acad. Sci.*, 2020. **117**(14): p. 7606-7612.
94. Zhang, E., et al., Fatigue fracture of nearly elastic hydrogels. *Soft Matter*, 2018. **14**(18): p. 3563-3571.
95. Zhang, W., et al., Fracture toughness and fatigue threshold of tough hydrogels. *ACS Macro Lett.*, 2018. **8**(1): p. 17-23.
96. Zhang, W., et al., Fatigue of double-network hydrogels. *Eng. Fract. Mech.*, 2018. **187**: p. 74-93.
97. Lake, G.J. and P.B. Lindley, The mechanical fatigue limit for rubber. 1965. **9**(4): p. 1233-1251.
98. Wallmersperger, T., et al., Multiscale modeling of polymer gels—chemo-electric model versus discrete element model. *Mech. Adv. Mater. Struct.*, 2008. **15**(3-4): p. 228-234.

99. Wallmersperger, T., B. Kroplin, and R. Gulch, Modelling and analysis of chemistry and electromechanics, electroactive polymer (eap) actuators as artificial muscles-reality, potential, and challenges, vol. *PM*. **136**: p. 335-362.
100. Wallmersperger, T., *Modellierung und simulation stimulierbarer polyelektrolytischer gele*. 2003: VDI-Verlag.
101. Hüther, A., X. Xu, and G. Maurer, Swelling of n-isopropyl acrylamide hydrogels in water and aqueous solutions of ethanol and acetone. *Fluid Ph. Equilibria*, 2004. **219**(2): p. 231-244.
102. Rubinstein, M. and R.H. Colby, *Polymer physics*. Vol. 23. 2003: Oxford university press New York.
103. Flory, P.J. and J.R. Jr., Statistical mechanics of cross‐linked polymer networks ii. Swelling. *J. Chem. Phys.*, 1943. **11**(11): p. 521-526.
104. Treloar, L.R.G., The physics of rubber elasticity. 1975.
105. Chen, H., et al., A comparative study of the mechanical properties of hybrid double-network hydrogels in swollen and as-prepared states. *J. Mater. Chem. B*, 2016. **4**(35): p. 5814-5824.
106. Kundu, S. and A.J. Crosby, Cavitation and fracture behavior of polyacrylamide hydrogels. *Soft Matter*, 2009. **5**(20): p. 3963-3968.
107. Li, Z., et al., The effect of water content on the elastic modulus and fracture energy of hydrogel. *Extreme Mech. Lett.*, 2020. **35**.
108. Zhang, W., et al., Fatigue-resistant adhesion i. Long-chain polymers as elastic dissipaters. *Extreme Mech. Lett.*, 2020. **39**: p. 100813.
109. Lin, S., et al., Muscle-like fatigue-resistant hydrogels by mechanical training. *Proc. Natl. Acad. Sci.*, 2019. **116**(21): p. 10244-10249.
110. Xiang, C., et al., Stretchable and fatigue-resistant materials. *Mater. Today*, 2020. **34**: p. 7-16.
111. Lin, S., et al., Anti-fatigue-fracture hydrogels. *Sci. Adv.*, 2019. **5**(1): p. eaau8528.